AN ABSTRACT OF THE THESIS OF

Ruiqing Ye for the degree of Doctor of Philosophy in
Electrical and Computer Engineering presented on June 13th, 2012 .

Title: Ultra-wideband Indoor Localization Systems

Abstract approved: ______________________________________

Huaping Liu

Indoor localization systems have a variety of applications such as tracking of assets, indoor robot navigation, and monitoring of people (e.g. patients) in hospitals or at home. Global positioning system (GPS) offers location accuracy of several meters and is mainly used for outdoor location-based applications as its accuracy degrades significantly in indoor scenarios. Wireless local area networks (WLAN) have also been used for indoor localization, but the accuracy is too low and power consumption of WLAN terminals is too high for most applications. Ultra-wideband (UWB) localization is superior in terms of accuracy and power consumption compared with GPS and WLAN localization, and is thus more suitable for most indoor location-based applications [1–4].

The accuracy and precision requirements of localization systems depend on the specific characteristics of the applications. For example, centimeter or even millimeter localization accuracy is required for dynamic part tracking, while decimeter accuracy might be sufficient for tracking patients in hospitals or at home. Note that accuracy is not the only aspect of the overall performance of the

system. Factors such as cost, range, and complexity should also be considered in system design.

In the first part of this dissertation, a centimeter-accurate UWB localization system is developed. The technical challenges to achieve centimeter localization accuracy are investigated. Since all the receivers are synchronized through wire connection in this system, a wireless localization system with centimeter accuracy is introduced in order to make the system easier for deployment. A two-step synchronization algorithm with picosecond accuracy is presented, and the system is tested in a laboratory environment.

The second part of this dissertation focuses on reducing the complexity of UWB localization systems when the localization accuracy requirement is relaxed. An UWB three-dimensional localization scheme with a single cluster of receivers is proposed. This scheme employs the time-of-arrival (TOA) technique and requires no wireless synchronization among the receivers. A hardware and software prototype that works in the 3.1-5.1 GHz range is constructed and tested in a laboratory environment. An average position estimation error of less than 3 decimeter is achieved by the experimental system.

This TOA scheme with receivers in a single unit requires synchronization between the transmitter and the receiver unit. In order to further reduce system complexity, a new time-difference-of-arrival localization scheme is proposed. This scheme requires multiple units, each operating on its own clock. It avoids synchronization between the transmitter and receivers, and thus makes the development of the transmitter extremely simple. The performance of this system is simulated and analyzed analytically, and turns out to be satisfactory for most indoor localization applications.

# Ultra-Wideband Indoor Localization Systems

by

Ruiqing Ye

A THESIS

submitted to

Oregon State University

in partial fulfillment of
the requirements for the
degree of

Doctor of Philosophy

Presented June 13th, 2012
Commencement June 2013

Doctor of Philosophy thesis of Ruiqing Ye presented on June 13th, 2012 .

APPROVED:

---

Major Professor, representing Electrical and Computer Engineering

---

Director of the School of Electrical Engineering and Computer Science

---

Dean of the Graduate School

I understand that my thesis will become part of the permanent collection of Oregon State University libraries. My signature below authorizes release of my thesis to any reader upon request.

---

Ruiqing Ye, Author

# ACKNOWLEDGEMENTS

I would have never been able to finish my dissertation without the guidance of my advisor, help from my friends, and support from my family.

I would like to express my deepest gratitude to my advisor, Prof. Huaping Liu, for his excellent guidance, invaluable advice and continuous encouragement. Without his help, I cannot finish this dissertation successfully. I am also very thankful to his understanding and caring to my study and life.

I am deeply indebted to Dr. Patrick Chiang, Dr. Thinqh Nguyen, Dr. Raviv Raich, and Dr. David Roundy for their great efforts and significant amount of time to serve on my Ph.D. committee.

I would like to thank Stephen Redfield, Johannes Huschle, Arash Abbasi and Seungjin Bake for many useful discussions and help on the Boeing project. I also want to thank my friends Jing Ju, Wei Liu, Jinjin He, Weiting Chen and many others for their precious friendship.

I would like to thank my parents, my sister and my brothers. They are always supporting me and encouraging me with their best wishes.

Finally, I would like to express my deepest love and appreciation to my husband, Ruliang Liao, who is always there cheering up me and stood by me through the good times and bad times.

# TABLE OF CONTENTS

# TABLE OF CONTENTS (Continued)

# TABLE OF CONTENTS (Continued)

# LIST OF FIGURES

## LIST OF FIGURES (Continued)

LIST OF FIGURES (Continued)

# LIST OF FIGURES (Continued)

# LIST OF TABLES

Table Page

# Chapter 1 – Introduction

## 1.1 Overview

Due to its large bandwidth, ultra-wideband (UWB) impulse radio has a high time resolution and is widely used in numerous indoor localization applications such as robot navigation [1], patients and high-value assets tracking in hospital [5, 12, 28] and smart audio-visual guides at museums, etc. Many localization systems using impulse UWB radio have been reported in both commercial products [5–7] and academic reports [8–11] with various localization accuracies from decimeter to centimeter.

The accuracy and precision requirements of different localization systems depend on the specific characteristics of the applications. For example, centimeter or even millimeter localization accuracy is required for dynamic part tracking, while decimeter accuracy might be sufficient for tracking patients in hospitals or at home. In addition to accuracy, cost, range, and complexity should also be considered in system design. This dissertation focuses on developing algorithms and new architectures of UWB localization systems under different accuracy requirements and system complexity constraints.

## 1.2 Summary of Contribution

We first develop a centimeter accuracy UWB three-dimensional (3-D) localization system for tracking miniature mechanical parts in an airplane wheel-well [12]. The major technical challenges to implement such a high precision localization system are analyzed. A new range estimation method is proposed to reduce the effect of path-overlap. Both simulation and experimental results show that the proposed method can effectively reduce the path-overlap effect and outperforms other range estimation methods such as first peak (FP) method [14] and search-subtract-and-readjust (SSR) method [15].

Besides range estimation accuracy, the receiver geometric configuration is another major factor that affects the localization accuracy of a TDOA localization system. Geometric dilution of precision (GDOP) is used to evaluate the effect of receiver geometric configuration on localization accuracy [16, 51]. Yang and Scheuing [17, 18] proposed an analytical solution to optimize the receiver geometric configuration by minimizing the Cramér-Rao lower bound (CRLB) for TDOA localization assuming a fixed source location. Schroeder [19] extended the theoretical optimum receiver placement to practical applications by minimizing the average GDOP. We first analyze how GDOP varies with different receiver geometric configurations. Assuming a near-optimum receiver geometric configuration, we then derive GDOP as a function of the number of receivers [20]. Finally, we simulate the position error bound (PEB) with different signal bandwidths and different numbers of receivers using the UWB indoor distance measurement error model. The results are useful to guide system design in optimizing the choices of signal bandwidth and the number of receivers to achieve a certain localization accuracy.

In order to make the system easier to deploy, a wireless localization system is prefered. One of the major challenges of implementing a wireless localization system is the synchronization between the receivers. Picosecond (ps) synchronization accuracy is required to achieve centimeter localization accuracy. Such a high synchronization accuracy makes the system design very challenging. The highest accuracy of UWB wireless indoor localization is reported recently in [57], in which an accuracy of 22 centimeters is presented. This system is claimed to be a wireless system because all the receivers are running on their own clocks. However, wire connection is still required for the data transfer from the receivers to the main processor. We present a wireless prototype localization system with centimeter accuracy using TDOA method. The basic concept of this system is introduced and a two-step synchronization method is proposed. An experiment is conducted in a laboratory environment, which shows the potential of the system for achieving a centimeter accuracy in an indoor environment.

The analysis above is based on the development of a centimeter-accurate localization system. Such a system requires distributed receivers, and synchronization of receivers is the major technical challenge that has not been fully resolved yet. The second part of this dissertation focuses on developing new architectures to reduce the complexity of UWB localization systems when the localization accuracy requirement is relaxed.

We first develop and analyze a 3-D UWB localization system that employs a single cluster of receivers placed in proximity (e.g., on a two-dimensional (2-D) plane within a few decimeters). This system employs TOA technique, and since the receivers are placed in proximity, the system does not need to synchronize the receivers wirelessly, resolving one of the major technical challenges for conventional TOA schemes with distributed receivers. We analyze optimum receiver placement in the sense of minimum estimation variance defined by the CRLB derived under the assumption of additive white Gaussian noise (AWGN) distortion, and derive the PEB as a function of the number of receivers and the distance between the source and the receiver unit. We also construct a hardware and software prototype that works in the 3.1-5.1 GHz range, and test it in a laboratory environment. We show, with experimental results, that with four receivers placed within a rectangle of $85 \times 70$ $cm^2$, the average position estimation error for sources that within 10 meters from the receiver unit is about 26.6 cm.

In order to further simplify the transmitter design and avoid wireless clock synchronization between the transmitter and receivers, a new multiple-unit TDOA localization scheme is proposed. The CRLB of this system is derived and the performance of this system with different receiver configurations and receiver unit sizes is analyzed. Simulation results show that the new system has potential to achieve a decimeter accuracy.

## 1.3 Dissertation Outline

Chapter 2 provides an overview of UWB signal and regulation, and summarizes common positioning technologies.

In Chapter 3, we introduce a pulsed UWB 3-D localization system with TDOA technology, which is implemented and tested in a metal-enclosed space. We describe the environment, system hardware/software implementation, test results, and the challenges toward achieving centimeter-accuracy in such an environment. We then analyze the effect of antenna-orientation-dependent pulse distortion on range estimation error. We also analyze the effect of multipath overlap in a metal-enclosed environment. A new range estimation method is proposed and evaluated through simulation and experiments.

In Chapter 4, the GDOP of TDOA localization when the receiver geometric configurations are near optimum is analyzed. The analytical relationship between the GDOP and the number of receivers is derived. The PEB as a function of the signal bandwidth and the number of receivers based on the UWB distance error model derived from measurement results is simulated.

In Chapter 5, we present a wireless prototype localization system with centimeter accuracy using the TDOA method. The basic concept of this system is introduced and a two-step synchronization method is proposed. Experiments are conducted in a laboratory environment, which show the potential of the system to achieve centimeter localization accuracies in an indoor environment.

In Chapter 6, an UWB 3-D localization system with a single cluster receivers using TOA technique is analyzed. The optimum receiver placement in the sense of minimum estimation variance defined by the CRLB is derived. A hardware and software prototype that works in the 3.1-5.1 GHz frequency band is constructed and tested in a laboratory environment.

In Chapter 7, we propose a new multiple-unit TDOA localization scheme that does not require wireless synchronization of the transmitter and the receiver. The CRLB of this system is derived and the performance of this system with different receiver configurations and different receiver unit size is analyzed

Chapter 8 gives conclusions and future work.

## 1.4 Notation

| | |
|---|---|
| $\approx$ | approximately equal to |
| $\|.\|$ | $\ell_2$ norm |
| $\mathrm{Tr}(\cdot)$ | the trace of a matrix |

## 1.5 Abbreviations

| | |
|---|---|
| 2-D | Two-dimensional |
| 3-D | Three-dimensional |
| AOA | Angle of arrival |
| AWG | Arbitrary waveform generator |
| AWGN | Additive white Gaussian noise |
| CRLB | Cramér-Rao lower bound |
| DAU | Data-acquisition unit |
| DME | Distance measurement error |
| EIRP | Effective isotropically-radiated power |
| FCC | Federal Communications Commission |
| FP | First peak |
| GDOP | Geometric dilution of precision |
| GPS | Global positioning system |
| LE | Leading edge |
| LNA | Low noise amplifier |
| MF | Matched filter |
| ML | Maximum likelihood |
| MPC | Multipath component |
| NLOS | Non-line-of-sight |
| ns | Nanosecond |
| PEB | Position error bound |
| ps | Picosecond |
| RMSE | Root mean square error |
| RSS | Received signal strength |
| SSR | Search subtract and readjust |
| sync node | synchronization node |
| TDOA | Time difference of arrival |
| TOA | Time of arrival |
| UWB | Ultra-wideband |

# Chapter 2 – Ultra-wideband Signals and Position Estimation Techniques

This chapter provides an overview of UWB signals and basic positioning techniques. The definition and regulation of UWB signals are introduced. Basic positioning schemes such as received signal strength (RSS), angle of arrival (AOA), TOA and TDOA are summarized in this chapter.

## 2.1 Definition of UWB

Early names for UWB technology include baseband, carrier-free, non-sinusoidal and impulse. The term UWB was coined by the US Department of Defense in the late 1980s [2]. According to the definition of US Federal Communication Commission (FCC), a signal is called UWB if it has an absolute bandwidth of at least 500 MHz, or a fractional bandwidth larger than 0.2 [22]. The absolute bandwidth is calculated as the difference between the upper frequency $f_H$ of the $-10$ dB emission point and the lower frequency $f_L$ of the $-10$ dB emission point, which is also called $-10$ dB bandwidth, as shown in Fig. 2.1.

$$B = f_H - f_L. \tag{2.1}$$

On the other hand, the fractional bandwidth is defined as

$$B_{frac} = \frac{B}{f_c} \tag{2.2}$$

where $f_c$ is the center frequency given by

$$f_c = \frac{f_H + f_L}{2}. \tag{2.3}$$

From Eqs. (2.1) and (2.3), the fractional bandwidth $B_{frac}$ can be expressed as

$$B_{frac} = \frac{2(f_H - f_L)}{f_H + f_L}. \tag{2.4}$$

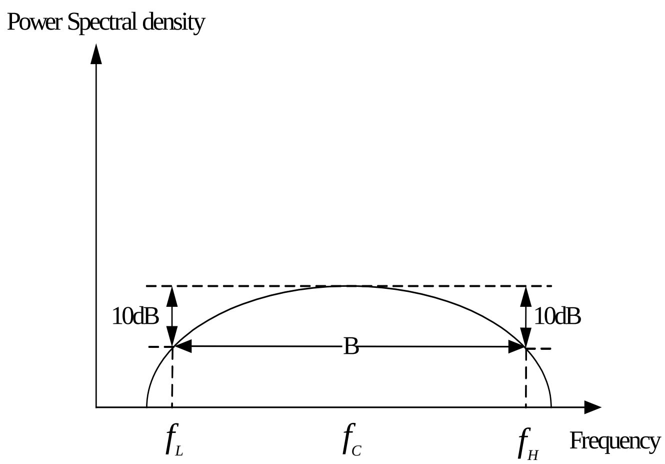


Figure 2.1: An UWB signal is defined to have an absolute bandwidth $B \geq 500$ MHz, or a fractional bandwidth greater than 0.2.

According to the FCC, an UWB system with $f_c$ higher than 2.5 GHz must have an absolute bandwidth larger than 500 MHz, and an UWB system with $f_c$ lower than 2.5 GHz must have a fractional bandwidth larger than 0.2.

Due to their large bandwidth, pulsed UWB systems are characterized by very short duration waveforms, usually in the range of nanoseconds (ns). A type of UWB communications system that transmits UWB pulses with a low duty cycle is called the impulse radio [23]. The large bandwidth of UWB systems brings many advantages for positioning, communications and radar applications. The main advantages can be summarized as follows:

- Good ability to penetrate through obstacles;
- High ranging, hence positioning accuracy;
- High-speed communications over short distances;
- Low power consumption.

The penetration capability of an UWB signal is due to the large frequency spectrum that includes low frequencies as well as high frequencies. The large bandwidth also results in a high time-resolution, which improves the ranging accuracy. According to the Shannon capacity formula, over an AWGN channel, the maximum data rate increases with bandwidth as

$$C = B \log_2(1 + SNR) \tag{2.5}$$

where SNR is the signal-to-noise ratio.

## 2.2 FCC Regulations for UWB Signals

Since UWB signals occupy a very large spectrum, they need to coexist with the incumbent systems without causing significant interference.

The FCC specifies the power emission limits for various types of UWB systems in terms of effective isotropically-radiated power (EIRP), which is defined as the product of the power supplied to an antenna and its gain in a given direction relative to an isotropic antenna. According to FCC regulations, the maximum EIRP in the range of $3.1 - 10.6$ GHz in any direction should not exceed $-41.3$ dBm/MHz [24]. In other frequency ranges, the FCC limits are different for different applications. For indoor and outdoor UWB communication systems, the FCC limits are shown in Fig. 2.2.

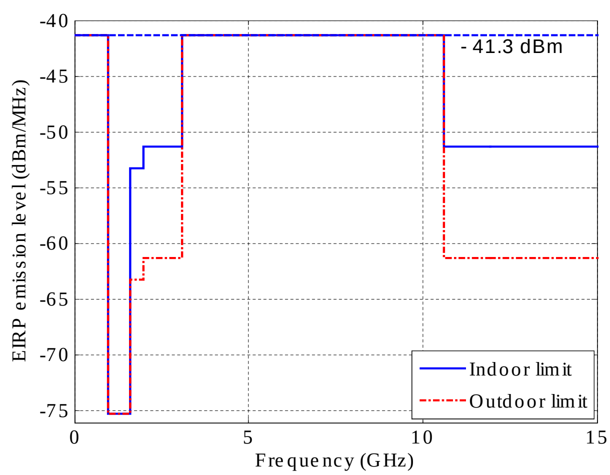


Figure 2.2: FCC emission limits for indoor and outdoor UWB communication systems.

The only difference in limit between the outdoor and indoor system is that the emission for outdoor systems in the frequency band from 1.61 to 3.1 GHz and 10.6 to 15 GHz should have an extra attenuation of 10 dB compared to that of indoor systems.

Besides the FCC emission limit, there are some other common FCC regulations for all the UWB systems [22, 25].

- The frequency $f_M$ at which the highest power is emitted must be within the $-10$ dB absolute signal bandwidth.
- Peak emissions within a 50 MHz bandwidth around $f_M$ may not exceed 0 dBm EIRP.
- Operation on aircraft, ship, or satellite is not permitted.

## 2.3 Position Estimation Techniques

In this section, common UWB positioning techniques are reviewed. The first step to estimate the position of a target node in a wireless network is to measure the signal parameters between the target node and the reference nodes. Different measurement techniques are discussed in the following subsections, including their principles, advantages and disadvantages.

### 2.3.1 Received Signal Strength

RSS technique provides distance information between two nodes by measuring the power of the received signal. The average received signal power decays proportionally to $d^{-n}$, where $n$ is the path-loss exponent, and $d$ is the distance between the two nodes. The path-loss model is expressed as

$$\bar{P}(d) = p_0 - 10n \log_{10}(d/d_0) \tag{2.6}$$

where $\bar{P}(d)$ is the average received signal power (dBm) at a distance $d$, and $p_0$ is the average received signal power (dBm) at a reference distance $d_0$. Although the path-loss model looks simple, in practical environments, the path-loss exponent is hard to estimate because of complex propagation mechanisms such as reflection, scattering and diffraction.

The CRLB for estimating distance using the RSS approach can be expressed as [26]

$$\sqrt{Var(\hat{d})} \geq \frac{ln10}{10}\frac{\sigma_{sh}}{n}d \tag{2.7}$$

where $\hat{d}$ represents an unbiased estimate of $d$ and $\sigma_{sh}$ is the standard deviation of the zero mean Gaussian random variable representing the log-normal shadowing effect. It is observed from (2.7) that the CRLB increases as the standard deviation of shadowing increases. Furthermore, a larger path-loss exponent results in a better estimation accuracy, as the average power becomes more sensitive to distance for a larger $n$. However, the CRLB does not change as the bandwidth of the signal changes. In other words, using RSS measurement cannot achieve accurate range estimation in UWB systems.

### 2.3.2 Angle of Arrival

Angle of arrival (AOA) is defined as the angle between the propagation directions of the incident waveforms. Each AOA measurement forms a radial line from the reference node to the target node to be positioned. In 2-D positioning, the estimated position of the target node is the intersection of two directional lines of bearing as shown in Fig. 2.3.

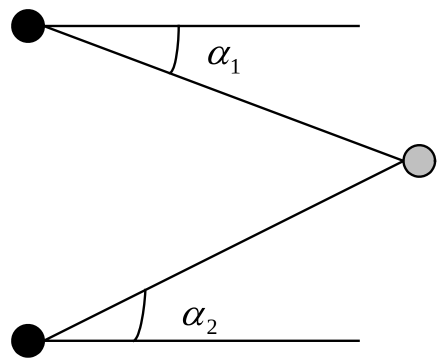


Figure 2.3: Two reference nodes (black dots) measure the angles between themselves and the target node (gray dot).

Antenna arrays are commonly employed to measure the AOA of an incident signal. The main idea behind AOA estimation via antenna array is that the difference of the arrival times at different antenna elements contains the angle (phase) information for a known geometry [2]. For a narrow band signal, whose bandwidth is much smaller than its center frequency, the time delay is related to the phase delay. For an UWB signal, however, because of the large bandwidth, the time delay could not be represented as a unique phase. Furthermore, using antenna arrays increases the system cost, annulling one of the advantages of UWB radio equipped with low-cost transceivers.

### 2.3.3 Time of Arrival

The TOA approach measures the time of flight from the target node to the reference node. The travel distance is the product of TOA and the speed of light $c$, which equals 299792458 m/s. Each TOA measurement forms a circle representing the distance between the target node and the reference nodes. To decide a target's position in 2-D positioning, the minimum number of TOA measurements is three as shown in Fig. 2.4.

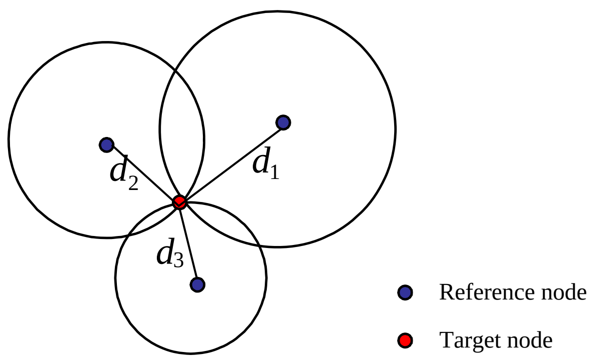


Figure 2.4: TOA positioning principle.

To estimate the TOA unambiguously, the clocks of the target node and reference nodes must be synchronized. Otherwise, huge ranging errors could occur since a 1 ns of clock error will result in 30 cm of range estimation errors.

For a single-path AWGN channel, the CRLB of the TOA measurement error is shown to be [27]

$$var(\hat{\tau}) \geq \frac{1}{8\pi^2\beta^2 SNR} \tag{2.8}$$

where $\hat{\tau}$ represents an unbiased TOA estimate and $\beta$ is the effective signal bandwidth defined in Eq. (2.9) as

$$\beta = \left( \frac{1}{E} \int_{-\infty}^{\infty} f^2 \left| S(f) \right|^2 \right)^{1/2} \tag{2.9}$$

where $S(f)$ is the Fourier transform of the transmitted signal and $E$ denotes the energy of the signal.

Note that from Eq. (2.8), the accuracy of TOA measurement increases as the SNR and the effective signal bandwidth increase. Therefore, due to the large bandwidth, UWB signals could yield a very accurate distance estimation using the TOA approach. The relationship between the effective bandwidth and the minimum standard deviation of the distance estimation is shown in Fig. 2.5.

It is observed from Fig. 2.5 that the theoretical limits are on the order of a few centimeters for reasonable SNR values, which indicates the high precision potential of UWB positioning based on TOA approach. Furthermore, a larger bandwidth results in better distance estimation, as expected.

### 2.3.4 Time Difference of Arrival

TDOA is the difference in time at which the signal traveling from the target node arrives at two different reference nodes. TDOA technique requires synchronization of the reference nodes' clocks. However, unlike TOA, clock synchronization between the target node and the reference nodes is not required, which makes

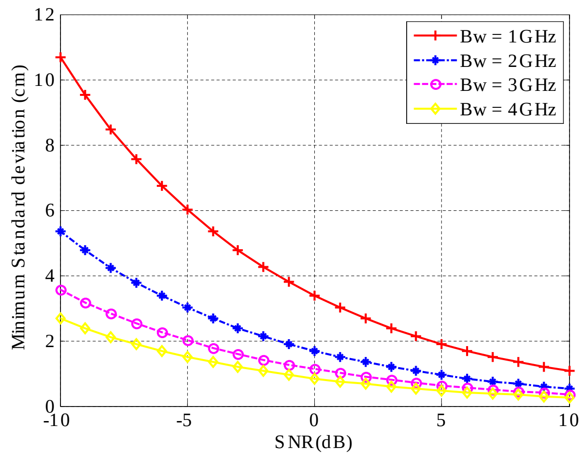


Figure 2.5: The minimum standard deviation of range estimation versus SNR for different signal effective bandwidth.

the system implementation simpler. One way to obtain a TDOA is to estimate TOA at each reference node and then calculate the difference between any two estimates. Let $t_1$, $t_2$ be the TOA measured in the corresponding reference nodes, and $t_0$ the transmission time of the signal from the target node. Since there is no synchronization between the target node and the reference nodes, $t_0$ is unknown. The distance difference between the target node and the two reference nodes are given by

$$d_1 = c(t_1 - t_0) \tag{2.10a}$$

$$d_2 = c(t_2 - t_0) \tag{2.10b}$$

$$d_{1,2} = d_2 - d_1 = c(t_2 - t_1). \tag{2.10c}$$

Each TDOA measurement defines a hyperbola passing through the target node with foci at the reference nodes. The principle of TDOA positioning is shown in Fig. 2.6.

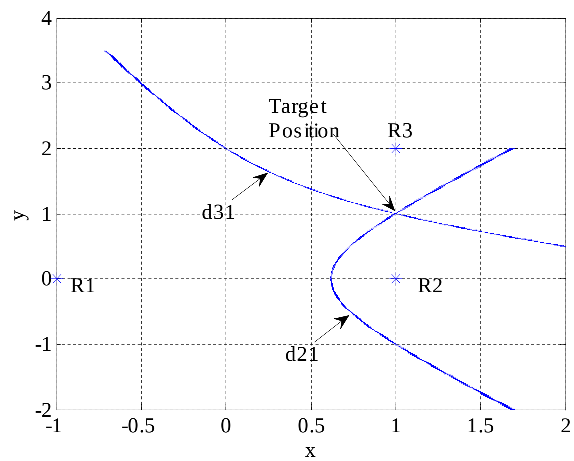


Figure 2.6: TDOA positioning principle

For 2-D positioning with three reference nodes, two independent hyperbolas can be formed and the intersection of the hyperbolas is the position of the target node. Since TDOA estimation depends on TOA estimation, its accuracy also increases as the signal bandwidth increases. In addition, TDOA does not require clock synchronization between the target node and the reference nodes, which makes the transmitter design much simpler than in TOA system. Therefore, TDOA approach is also a good candidate for UWB localization.

## 2.4 Conclusion

In this chapter we first presented a background of UWB signal and the FCC regulation of UWB communication systems. Then the fundamentals of UWB positioning technologies were described.

# Chapter 3 – High-precision Ultra-wideband Localization System: Implementation and Challenge

## 3.1 Introduction

The availability of a robust, high-precision, 3-D indoor localization system could result in innovations in a variety of applications such as health care [28], asset tracking [5], and navigation for indoor robots [1].

An example of such applications is the automatic tracking of miniature mechanical parts in an airplane wheel-well using UWB localization. In the wheel-well there are hundreds to thousands of nuts that must be tightened to an exact torque level. Many of these nuts are within an inch of distance from one another. Tightening these nuts is often completed at different times and by different engineers. Currently this is done manually as well as manual recording of information such as who had worked on which ones, the time completed and exact torque levels. The work is error-prone, tedious, and extremely time consuming.

An automatic book-keeping system could result in tremendous time and cost savings and significantly increased reliability. This is best achieved by deploying a high-precision localization system with sensing (e.g. torque values, temperature, humidity, vibration, etc.) and wireless data transmission capabilities. The first version of our system focuses on localizing the B-nuts position in the wheel-well. Implementing such a system in the harsh metal environment faces a lot of challenges including: pulse dispersion caused by the antennas, range estimation error caused by the severe multipath interference, sampling rate limit, etc. Errors associated with these issues need to be carefully considered for a system design.

In this chapter, we present a centimeter-accurate, 3-D localization experiment system using pulsed UWB radio that we developed and tested in a dense multipath environment−a metal enclosed space with substantial metallic objects inside. From the measurement results, we observe two major technical challenges toward realizing a robust, high-precision localization system: one is the distortion of the received waveform when the boresights of the transmit and receive antennas are not aligned and the other is path-overlap caused by multipath. For various relative angles of the transmit and receive antenna boresights, we measure the received pulse shapes and compare them with the ideal one, enabling clear assessment of the distortion caused by the radiation subsystem. Although the exact causes of such angle-dependent pulse distortion are not clear, the antenna is proved to be a major factor [29, 30]. It is, in principle, possible to derive distortion-free conditions for antennas [29], but in practice, such antennas are not very practical to realize because of the wide bandwidth of the signal. We thus analyze the errors of the estimated distance caused by angle-dependent waveform distortion with three timing estimation approaches− FP [14] detection, Leading Edge (LE) detection [12], and Matched Filter (MF) approach. Although this is for a specific setting of the system and propagation environment, the results form a good baseline of the expected error for any general indoor settings. From the extensive experiments that we have conducted, we find that the occasional path-overlap is a major error source that reduces the robustness of a centimeter-accuracy localization system. Techniques for timing detection in the presence of path-overlap include FP and SSR [15]. For applications that require centimeter location accuracy, these methods are insufficient. Therefore, we proposed a new range estimation algorithm that outperforms these two methods and virtually eliminates the timing errors caused by path-overlap.

## 3.2 The Experimental System

We have developed and successfully tested a centimeter-accuracy pulsed UWB localization hardware and software prototype system, as shown in Fig. 3.1. The goal is to automatically track the locations of miniature mechanical parts,

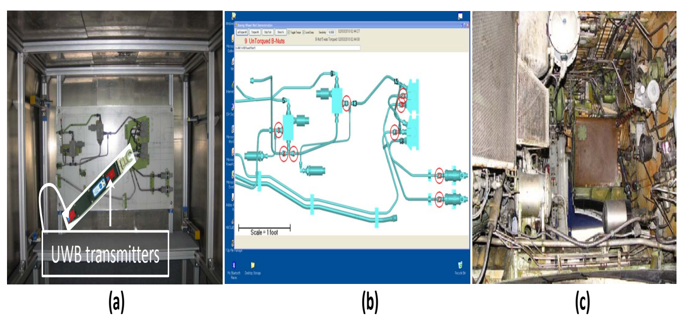


Figure 3.1: A centimeter-accuracy UWB localization system for tracking miniature mechanical parts (B-nuts) we have developed: (a) The metal-enclosed environment in which the system was tested. The closest parts successfully identified were about 2 centimeters apart; (b) Realtime display of the location of the B-nuts torqued by the wrench; (c) The actual Boeing 737 airplane wheel well where the prototype system was tested successfully.

mainly the B-nuts, and the torque values applied on a B-nut by a wrench. This is achieved by implementing two UWB transmitters in the wrench. The localization system tracks the locations of both transmitters when the wrench rotates around a B-nut. The moving trajectories of the two transmitters are then used to estimate the 3-D location of the B-nut. The system uses the 3.1-5.1 GHz frequency band, and the transmitted signal fits in the spectral mask for UWB signaling. The measured received signal is shown in Fig. 3.2.

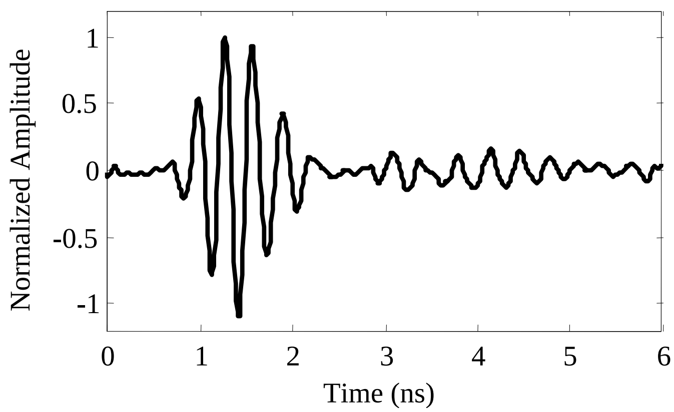


Figure 3.2: Received UWB pulse (amplitude is normalized).

The two transmitters on the same wrench work in a time-division fashion, and the transmitters and receivers use an omni-directional antenna described in [31]. The system implements TDOA algorithm, and employs four receivers, the minimum number of receivers required for 3-D localization with TDOA. The whole system block-diagram is shown in Fig. 3.3, where the functions inside the dashed box are implemented in software. The sampling module is realized by a high-speed sampling scope and all the receivers share a common clock, so the receiver synchronization error is not considered.

From the experiments we have observed two technical challenges toward realizing a robust, high-precision system: angle-dependent waveform distortion and path-overlap. Because of the ultra-wide bandwidth of the signals, the antennas

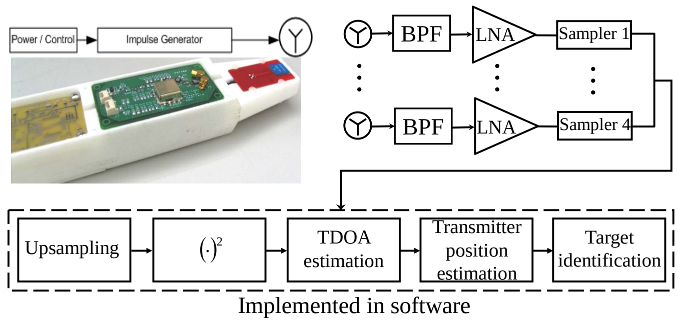


Figure 3.3: Block diagram of the experimental system.

inevitably cause a distortion to the received waveform [30,36–39]. This distortion is not fixed. It depends on the relative angle of the boresights of transmitting and receiving antennas, making the pulse recover difficult. Fig. 3.4 shows the measured received pulses with Fractus antennas: when ($\theta = 0^o, \phi = 0^o$), the received pulse is almost identical to the transmitted pulse (no distortion); at other relative angles, various levels of distortion are observed. We have experimented with two commercially available antennas, all of which exhibiting similar behaviors. While it is theoretically possible to derive distortion-free conditions for the antenna [29], it is not feasible to design such antennas in practice when size and efficiency are important concerns. It is difficult to obtain precise timing information from the location-varying, distorted waveforms, no matter what algorithms (e.g., LE detection, FP detection, etc.) are used. For *coarse* location resolutions (e.g., greater than 10 cm), such distortion might not matter. For the *ultra-high accuracy* required for some applications such as the one shown in Fig. 3.1, this error must be minimized or even eliminated.

## 3.3 Technical Challenges and Solutions

### 3.3.1 Angle-dependent waveform distortion

Antenna design [32] is one of the key aspects of UWB systems that has been widely investigated. Although in theory the antenna subsystem could act as an ideal bandpass filter, it is not the case in practice. The received pulses will be slightly distorted [30, 33, 34] because of the non-uniform gain across the signal band. Such distortion could be ameliorated to some extent through the use of pulse shaping filters or an appropriate template for correlation detection [35]. However, with practical antennas, the waveform distortion is dependent on the angle of radiation or reception [36], as the angular variation of the antenna pattern is typically frequency dependent.

In [33], performance of UWB antennas is studied theoretically. It concludes that no real UWB antenna can provide truly omnidirectional performance when pulse fidelity is considered. In [30], pulse distortion of rectangular-aperture antenna radiation is studied and its effect on the bit-error rate (BER) of a pulsed UWB communication system is analyzed. It shows that the BER of the system varies significantly when the signal is transmitted in different angles using a correlation receiver. In [34], the received signal waveform with different combinations of transmit and receive antennas is measured, and the performance of the pulse synchronization is investigated.

The performance of timing-based localization is highly dependent on the quality of TOA/TDOA measurements. TOA/TDOA estimation accuracy will be affected by the angle-dependent pulse distortion since receivers are located at different positions. Currently, it is not specifically clear how much angle-dependent pulse distortions affect the TDOA estimation accuracy. In this section, for a specific environment and system setup, we use our experimental data to evaluate this aspect.

The experimental system is shown in Fig. 3.4. The center frequency of a transmitted carrier-modulated Gaussian pulse is 4 GHz with a -10 dB bandwidth of 2 GHz. The transmitter and receivers use the Fractus antennas [31]. One receive antenna is in the boresight direction of the transmit antenna and is located 50 cm away. The other receive antenna is rotated to a different angle relative to the transmit antenna but is kept at a fixed distance of 50 cm to the transmit antenna.

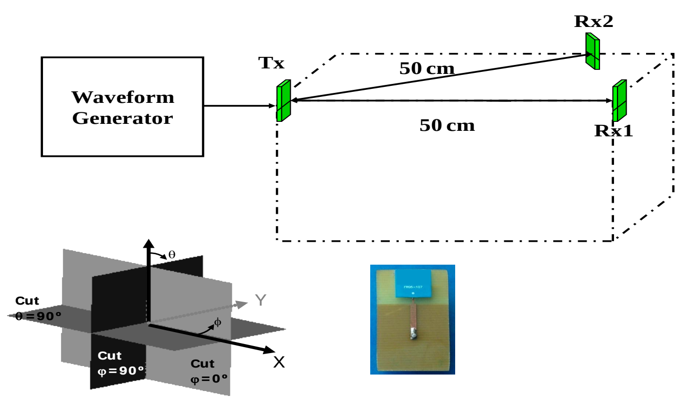


Figure 3.4: Experiment system setup for antenna analysis.

The received signal is sampled and processed in a computer. In order to reduce the noise effect, 100 pulses are averaged at each direction to form the final normalized pulse. The normalized received pulses from different angles are shown in Fig. 3.5. We observed that at $\theta = 100^o, \phi = 115^o$, the peak of the pulse is shifted and the pulse width is wider compared to the pulse received from the boresight direction.

In order to evaluate the effect of pulse distortion on TDOA estimation accuracy, we conducted 100 independent experiments. The Root-Mean-Square (RMS) error of TDOA estimation is calculated by using the FP detection method, the LE method [12], and the MF method. For the MF method, the template signal is the received signal in the boresight direction. The results for different angles are shown in Table 1.

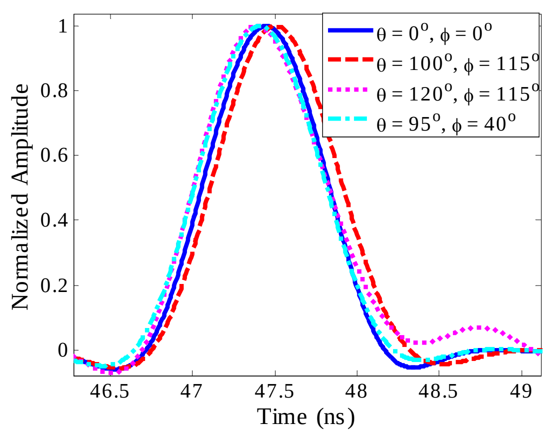


Figure 3.5: Received pulse shapes for different angles between the boresights of the transmit and receive antennas.

Table 3.1: RMS values of TDOA estimation error due to pulse distortion.

| Relative angles | FP | LE | MF |
|---|---|---|---|
| $\theta = 100^o, \phi = 115^o$ | 2.0292 cm | 1.4762 cm | 2.0564 cm |
| $\theta = 120^o, \phi = 115^o$ | 1.6861 cm | 1.9629 cm | 1.5015 cm |
| $\theta = 95^o, \phi = 40^o$ | 0.9205 cm | 1.3852 cm | 0.8683 cm |

From the results in Table 1, we see that for a realistic system setup, TDOA error resulting from pulse distortion is within the range of a couple of centimeters. For medium accuracies (e.g., greater than 10 cm), this is negligible. For centimeter-accuracy localization, this angle-dependent (thus transmitter location-dependent) error should be mitigated.

### 3.3.2 Path-overlap

In our experiment as shown in Fig. 3.1−a dense multipath scenario, we find that the first multipath often overlaps with the direct path, and thus significantly reduces the range measurement accuracy.

Fig. 3.6 shows one of the received signals (after conversion from 3.1-5.1 GHz to baseband) when the direct path overlaps with the first multipath.

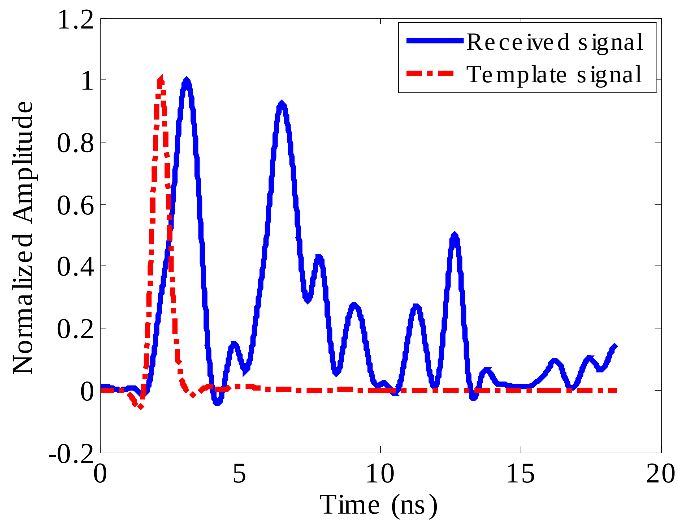


Figure 3.6: A sample of the measured received signal when the two first-arrival paths overlap.

In [40], the effect of path-overlap on the localization accuracy is analyzed theoretically and the path-overlap coefficient for different waveforms and propagation channels is evaluated. To mitigate this problem, a modified phase-only correlator method is proposed in [13] to estimate the TOA in the frequency domain. However, a clean template waveform is needed for this method, which is hard to obtain in a practical system. In [15], a SSR method is presented to reduce the range error caused by the irresolvable multipath. In [41], several TOA estimation methods are evaluated in an industrial LOS environment. However, the performance of these methods on minimizing the timing error caused by the path-overlap is not evaluated. In this section, we propose a new range estimation method and compare its performance with that of the FP detection method and the SSR method on reducing the path-overlap effect.

Before going through the proposed method, the basic concept of SSR method is introduced. The SSR method is modified from the FP method. The principle is shown as follows. After estimating the TOA corresponding to the strongest multipath component (MPC), this MPC (generated using the template signal) is subtracted from the received signal. In the next step, the TOA of the second strongest MPC is estimated using the updated received signal (after the strongest MPC is subtracted). Again this MPC is reconstructed, and subtracted from the updated signal. In [15], the process stops after doing $\tilde{N}$ times iteration, where it assumes that the number of MPC before the strongest path $\tilde{N}$ is known, which is hard to achieve in a practical system. Therefore, we set a threshold based on the SNR of received signal and stop the process when the strongest peak of updated signal is lower than the threshold.

The proposed method is modified based on the SSR method and is summarized as follows:

1) Use the SSR method in [15], estimate the first peak $t_p$ of the received signal envelop $y(t)$.

2) Determine a threshold value with respect to the first peak value

$$\lambda = \alpha \times y(t_p) \tag{3.1}$$

where $\alpha$ is the dynamic threshold factor. The value of $\alpha$ is usually set based on the signal-to-noise ratio of the system. In our simulation, $\alpha = 0.3$ is chosen.

3) Search backward from the first peak to locate the first $\hat{t}$ where the signal amplitude exceeds the threshold $\lambda$.

$$\hat{t} = f[y(t_p)] \tag{3.2}$$

where $f[\cdot]$ is a function to determine the leading edge for $y(t) > \lambda$.

We consider a simple case where the received waveform has only two paths. This simple scenario will provide insights into the effect of path-overlap on TOA/TDOA estimation. The template signal used in the simulation is an ideal baseband pulse received from the implemented system, which is shown in Fig. 3.6. The three algorithms are FP [14], SSR [15], and the proposed method.

Two factors affect the path-overlap coefficients: one is the relative amplitude of the overlapping multipath and the direct path, $\eta$, and the other is the delay between the multipath and the direct path, $\tau$ [40]. We will evaluate the impact of $\eta$ and $\tau$ when different range estimation methods are employed. First, we set

$\eta = 1$ and vary $\tau$ from 0 ns to 1.5 ns to calculate the TOA estimation. The range error using three different TOA estimation algorithms is shown in Fig. 3.7.

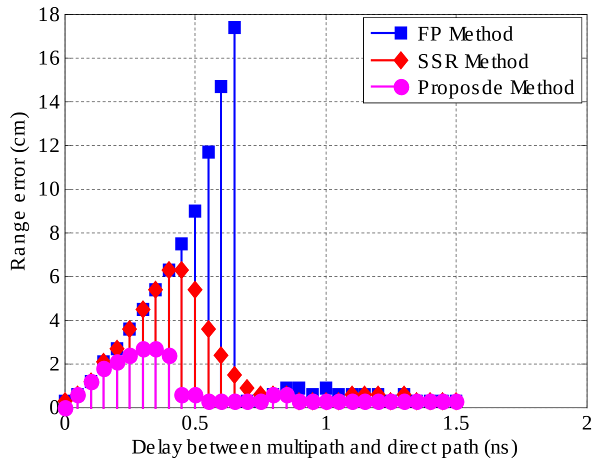


Figure 3.7: TOA estimation error versus the delay $\tau$ between direct path and multipath.

We draw three main conclusions from the simulation results: (1) The proposed method performs significantly better than the other two methods; (2) When $\tau \leq 0.4$ ns, SSR performs the same as the FP method. This means that the SSR method cannot separate the multipath when $\tau \leq 0.4$ ns; (3) For the FP method, the maximum TOA estimation error is 17.4 cm when $\tau = 0.65$ ns; for the SSR method, the maximum TOA estimation error is 6.3 cm when $\tau = 0.45$ ns; and for the proposed method, the maximum TOA error is 2.7 cm when $\tau = 0.35$ ns.

In order to evaluate the effect of the relative amplitude $\eta$ on TOA estimation error, we set $\tau = 0.3$ ns and $\tau = 0.5$ ns. Then we vary $\eta$ from 0.1 to 2 and observe the output. The simulation results are shown in Fig. 3.8 and Fig. 3.9.

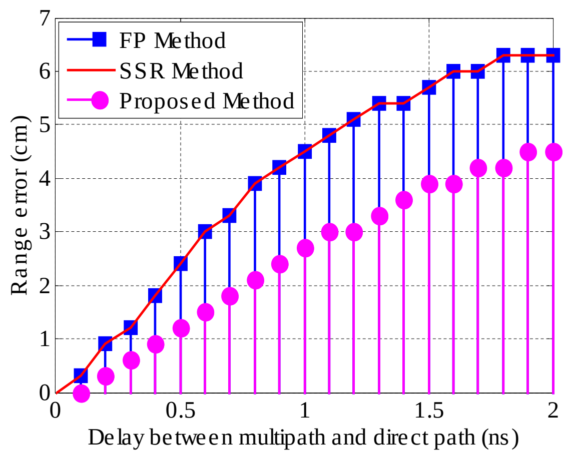


Figure 3.8: TOA estimation error versus the relative amplitude $\eta$ between direct path and multipath when $\tau = 0.3$ ns.

From Fig. 3.8 we notice that the SSR method performs the same as the FP method when $\tau = 0.3$ ns, which implies that the SSR method could not reduce the multipath error when $\tau < 0.4$ ns. The proposed method performs much better than the other two methods in both simulations. Without considering the noise effects, the proposed method has very good range estimation accuracy: less than 4 cm in all simulated cases.

## 3.4 Range Estimation Experiment

From the analysis results we have concluded that the proposed range estimation method outperforms the FP and SSR methods in the case when there are only two multipaths. In this section, a ranging experiment is conducted in an indoor

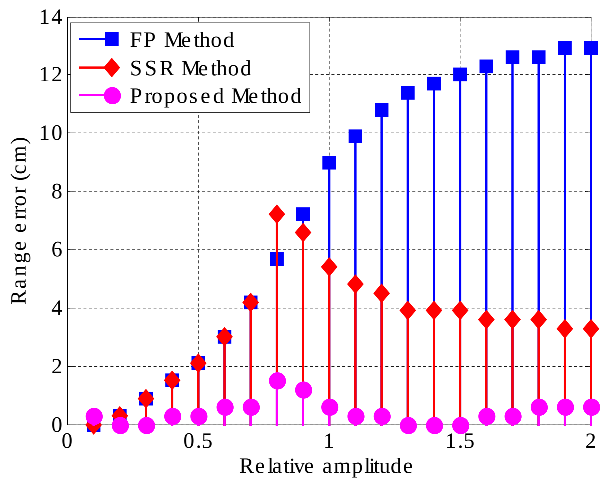


Figure 3.9: TOA estimation error versus the relative amplitude $\eta$ between direct path and multipath when $\tau = 0.5$ ns.

environment to further evaluate the performance of these three methods. The basic test diagram is shown in Fig. 3.10 and the test discription is shown as follows.

- One transmitter and one receiver
- Distances (feet from receiver) 21,22,23,24,25,50,75,100
- Height(feet from level) 0, +2 and -2
- Multiple readings (20) at each distance and height

### 3.4.1 Experiment Setup

A block diagram of the measurement apparatus is shwon in Fig. 3.11. It consists of an arbitrary waveform generator (AWG) that generates an UWB ideal

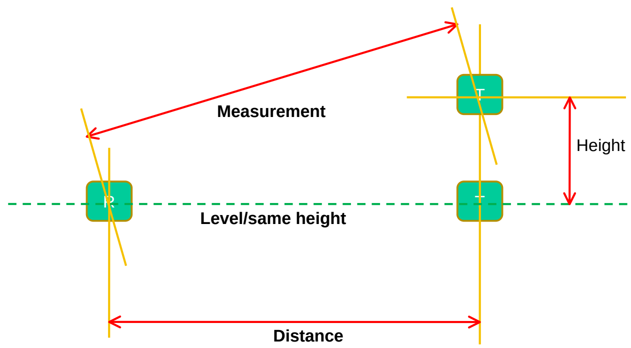


Figure 3.10: Basic test diagram for the range experiment.

Gaussian pulse with center frequency of 4 GHz and $-10$ dB bandwidth of 2 GHz. The pulse duration is about 1 ns and the pulse repetition time is 200 ns. An UWB omni-directional transmitting antenna is connected to the pulse generator via a long coaxial cable. The length of the coaxial cable is 50 feet. The receiver unit consists of a receiving omni-directional antenna, a wideband low noise amplifier (LNA), bandpass filter and a digital sampling scope.

The triggering signal from the AWG is used to trigger the sampling scope via a *fixed-length* coaxial cable. There is a fixed delay between the transmitter and receivers. Therefore, the transmitter and the receiver are synchronized by subtracting the reference delay.

The sampling scope has a maximum real-time sampling rate of 20 GHz, which has a sampling duration of 50 ps, and it has the capability to average over several received waveforms for noise reduction purposes. Taking advantage of this capability, 20 sequentially received pulses are averaged and recorded to the computer through an Ethernet cable.

The digital data is first upsampled to 100 GHz to increase the time resolution to 10 ps, then it goes through a square-law device and a low pass filter to recover the baseband pulse.

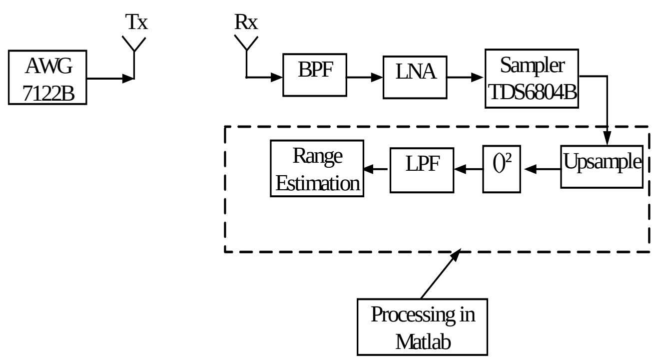


Figure 3.11: Block diagram of the measurement apparatus.

### 3.4.2 Experiment Result

The measurements are made in the corridor of a building shown in Fig. 3.12. The transmit and receive antennas are fixed in two metal stands. Besides the metal stands, there are other objects such as walls, doors, ceiling which can reflect or diffract the signal. The experiment environment is shown in Fig. 3.12

At each distance and height, 20 pulses are taken, and the RMSE of the distance estimations using FP, SSR and the proposed methods are calculated

Figure 3.12: Experiment Environment

by (3.3)

$$RMSE(\hat{d}) = \sqrt{\frac{1}{N}\sum_{i=1}^{N}(\hat{d}_i - d)^2} \tag{3.3}$$

where $\hat{d}_i$ is the $i$th distance estimation at the same point and $N = 20$ is the number of estimations at each point.

The experiment results are shown in Figs. 3.13 - 3.15.

It is noted from Fig. 3.13 that both the SSR method and the proposed method outperform the FP method. The maximum RMSE for FP detection method is about 0.7 feet at the distance of 21 feet, and the average RMSE of the FP detection method is 0.3452 feet. The proposed method performs better than the SSR method when the distance is smaller than 75 feet, and it is slightly worse than SSR method at distance of 75 feet and 100 feet. The average RMSEs for SSR method and the proposed method are 0.1475 feet and 0.1119 feet.

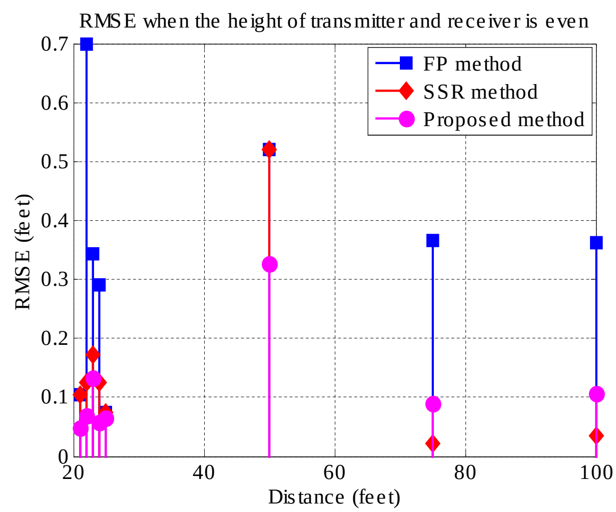


Figure 3.13: RMSE when the height of transmitter and receiver are even.

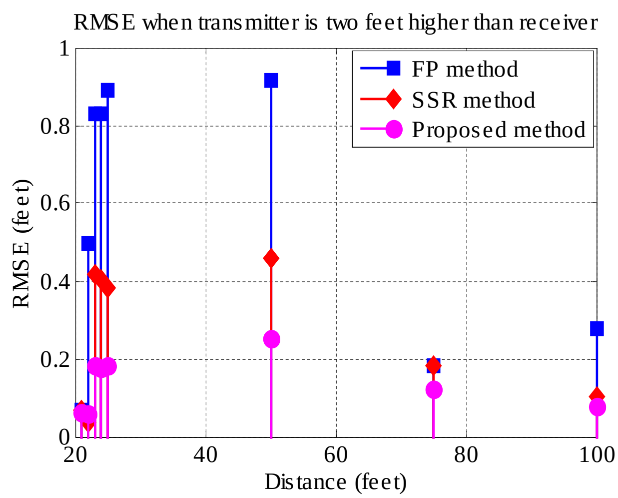


Figure 3.14: RMSE when transmitter is located at locations two feet above the receiver.

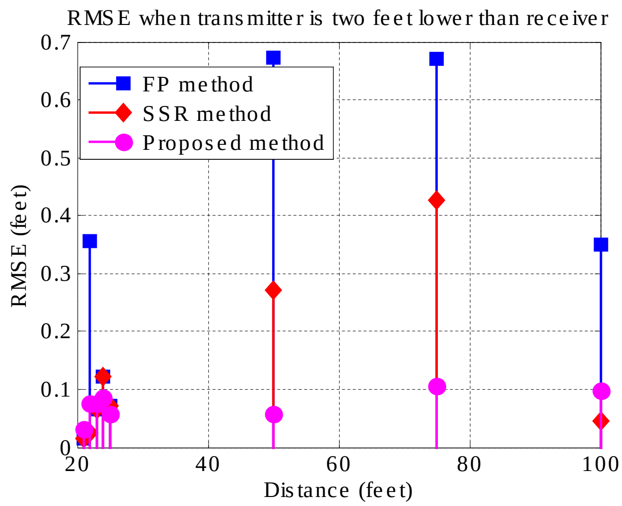


Figure 3.15: RMSE when the transmitter is located at locations two feet below the receiver.

In Fig. 3.14, the effect of multipath overlap on the distance estimation is severe. In this case, the performance of the proposed method is much better than that of the FP and SSR methods. For FP, SSR and the proposed method, the maximum RMSEs are about 0.92 feet, 0.46 feet and 0.25 feet, respectively, and the average RMSEs for these three methods are 0.56, 0.26 and 0.14 feet.

In Fig. 3.15, there is no multipath overlap at distances of 21, 23, 24, 25 feet, and all three range estimation methods perform similarly. However, when multipath overlap is present such as at distances such as 22, 50, 75 feet the proposed method performs much better than the other two methods. At the distance of 100 feet, the SSR method performs slightly better than the proposed method.

## 3.5 Conclusion

Using experimental results obtained from a centimeter-accuracy 3-D indoor localization system, we have studied the effect of angle-dependent pulse distortion caused by UWB antennas on the TOA/TDOA estimation error. We have shown that for medium to low location accuracies (e.g., greater than 10 cm), the error resulting from angle-dependent pulse distortion is negligible, regardless which range estimation methods are employed. For centimeter-accuracy localization, however, such error must be reduced. We have also investigated the effect of path-overlap that occurs in dense multipath environments. A new range estimation method is proposed to reduce the range estimation error caused by the path-overlap. Simulation results have shown that the proposed range estimation method significantly outperforms existing FP and SSR methods. Furthermore, a ranging experiment has been conducted in an indoor area, and the experiment result shows that the proposed method performs better than the SSR method and FP method, especially for cases when the multipath overlap is severe.

# Chapter 4 – UWB TDOA Localization System: Receiver Configuration Analysis

## 4.1 Introduction

The accuracy of TDOA localization systems depends mainly on two factors: receiver geometric configuration and TDOA/range estimation accuracy. Range estimation techniques have been well studied in [14, 15, 26, 42, 43]. The effect of receiver geometric configuration on localization accuracy is studied in [16, 51]. The GDOP [16] is commonly used to assess the effectiveness of different receiver geometric configurations. An assumption model for the GDOP calculation is that the range measurement errors are identically distributed. If this assumption is not satisfied, the PEB [51] that combines both receiver geometric configuration and the statistical properties of the range measurements could be used. While the effect of receiver geometric configuration on localization accuracy is well known, optimal receiver placement for TDOA localization is much less studied. Yang and Scheuing [17, 18] propose an analytical solution to optimize the receiver geometric configuration by minimizing the CRLB for TDOA localization assuming a fixed source location. Schroeder [19] extends the theoretical optimum receiver placement to practical applications by minimizing the average GDOP.

In the previous chapter, we have developed a centimeter-accurate UWB localization system. We find that besides the information about the near-optimal receiver geometric configuration, the minimum number of receivers required to achieve a certain accuracy is critical to guide system design. The main goal of the study is to determine the achievable location accuracy as a function of the signal bandwidth and the number of receivers assuming a near-optimum receiver geometric configuration. We first analyze how GDOP varies with different receiver geometric configurations. Assuming a near-optimum receiver geometric configuration, we then derive GDOP as a function of the number of receivers. Finally, we simulate the PEB with different signal bandwidths and numbers of receivers using the UWB indoor distance measurement error model. The results will be useful to guide practical system design in optimizing the choices of signal bandwidth and the number of receivers to achieve a certain localization accuracy.

## 4.2 TDOA Measurement Model

There are two widely used approaches for TDOA estimation. One is the cross-correlation method [44], which calculates the cross-correlation between two signals traveling from the transmitter to the receivers. This method does not work well in multipath environments and is thus not suitable for the indoor localization. In the other approach, the TOA/range between the transmitter and the receivers is estimated first based on the receiver local time. Then, the difference between the two TOA/range estimates is calculated assuming that all receivers are synchronized. This method, upon which the TDOA error model is built, is commonly used for indoor localization.

The estimated distance $\hat{d}_i$ between the transmitter and the $i$th receiver can be modeled as

$$\hat{d}_i = d_i + b_i + n_i = \|\mathbf{p} - \mathbf{q}_i\| + b_i + n_i, i = 1, \cdots, N \tag{4.1}$$

where $\|.\|$ denotes the $\ell_2$ norm, $d_i$ is the actual distance between the transmitter and the $i$th receiver, $b_i$ is a positive bias caused by the non-line-of-sight (NLOS) propagation, $n_i$ is a zero mean Gaussian variable with variance of $\sigma^2$, $\mathbf{p}$ is the position of the transmitter, $N$ denotes the total number of receivers, and $\mathbf{q}_i$ is the position of the $i$th receiver. For line-of-sight (LOS) cases, $b_i = 0$. The distance difference between the transmitter to the $i$th and $j$th receivers, which equals the product of TDOA and the speed of light, can be calculated by

$$\hat{d}_{i,j} = \hat{d}_i - \hat{d}_j = d_i - d_j + n_i - n_j = d_{i,j} + n_{i,j} \tag{4.2}$$

where $n_{i,j} = n_i - n_j$ is a zero mean Gaussian variable with variance of $2\sigma^2$. For a fixed transmitter and $N$ receivers, there are $N(N-1)/2$ distance difference estimates. However, only $N-1$ estimates are linearly independent; others can be calculated from these $N-1$ estimates. For example, $\hat{d}_{i,j} = \hat{d}_{i,1} - \hat{d}_{j,1}$ when $i, j > 1$.

The position estimation problem with the TDOA technique is actually a problem of solving a set of hyperbolic equations. Many methods can be used such as the Taylor-series expansion method [45] and CH method [46]. Receiver geometric configuration affects the localization accuracy. Optimum receiver geometric configurations for a given transmitter position have been derived by minimizing the CRLB [17]. The Platonic solids - tetrahedron, octahedron, cube, icosahedron, and dodecahedron - have been proven to be optimum geometric configurations when the transmitter is located at the center of these solids. Even though these solids are only optimum under some strict conditions, it is a good guidance for the practical system design.

## 4.3 Cramér-Rao Lower Bound for TDOA Localization

The CRLB is a lower bound for the variance of an unbiased estimator. It is often used as a benchmark for estimation performance. We let $\mathbf{d} = [\hat{d}_{2,1}, \hat{d}_{3,1}, ..., \hat{d}_{N,1}]$ denote the final TDOA estimates. Assuming that the TDOA estimation vector $\mathbf{d}$ is a multivariate Gaussian variable with mean vector $\boldsymbol{\mu}$ and covariance matrix $\mathbf{C}$, we write the CRLB as [52]

$$\mathbf{J}^{-1} = (\mathbf{G}\mathbf{C}^{-1}\mathbf{G}^T)^{-1} \tag{4.3}$$

where $\mathbf{J}$ is the Fisher information matrix, $\mathbf{C}$ is the covariance matrix, and $\mathbf{G} = [\mathbf{g}_{2,1}, \mathbf{g}_{3,1}, ..., \mathbf{g}_{N,1}]$ with

$$\mathbf{g}_{i,1} = \mathbf{g}_i - \mathbf{g}_1, \mathbf{g}_i = \frac{\mathbf{p} - \mathbf{q}_i}{\|\mathbf{p} - \mathbf{q}_i\|}. \tag{4.4}$$

From Eq. (4.4), it is observed that the CRLB does not depend on the range but the direction between the transmitter and the receiver since $\|\mathbf{g}_i\| = 1$. Note that the covariance matrix $\mathbf{C}$ is not a diagonal matrix since $\hat{d}_{i,1}$ and $\hat{d}_{j,1}$ are not independent.

With the CRLB, the PEB can be calculated as [51]

$$\mathrm{PEB}(\mathbf{p}) = \sqrt{tr\{\mathbf{J}^{-1}\}} \tag{4.5}$$

where $tr\{\cdot\}$ is the trace of a square matrix. The PEB is a fundamental limit on the accuracy of any unbiased localization method.

If the range estimates have the same distribution with variance of $\sigma^2$ (or $2\sigma^2$ for the estimates of the distance difference), the GDOP can be defined as

$$\mathrm{GDOP}(\mathbf{p}) = \mathrm{PEB}(\mathbf{p})/\sigma. \tag{4.6}$$

## 4.4 GDOP Versus the Number of Receivers

GDOP indicates the effectiveness of a geometric configuration. In this section, we analyze the relationship between the GDOP and the number of receivers. The receiver geometric configuration is shown in Fig. 4.1. The receivers are placed at the corners of a cube labeled $Rx1$ to $Rx8$. The order of the receiver placement is based on the optimum receiver geometric configuration derived in [17]. Thus, in our simulation, we call this configuration the near-optimum configuration. For example, $Rx1, Rx2, Rx3, Rx4$ form a tetrahedron and $Rx1, Rx2, \cdots, Rx8$ form a cube. However, the number of optimum receiver geometric configurations given in [17] is limited, and when the number of receivers is odd, an optimum configuration does not exist. Therefore, we evenly place the receivers at the corner for $Rx5$, $Rx6$, and $Rx7$ to ensure that it covers the largest area of the cube.

### 4.4.1 GDOP Simulation with the Transmitter at the Center

Five configurations with 4-8 receivers will be used for the simulation and analysis in this section. To simplify the analysis, we first let $n_i, i = 1, ..., N$, be zero mean Gaussian random variables with the same variance $\sigma^2$, and place the transmitter at the center of the cube. Since the optimum receiver geometric configuration given in [17] is derived from the assumption that the transmitter is at the center, we call the GDOP in this case the *optimum* GDOP. The simulation result of the *optimum* GDOP versus the number of receivers is given in Table 4.1.

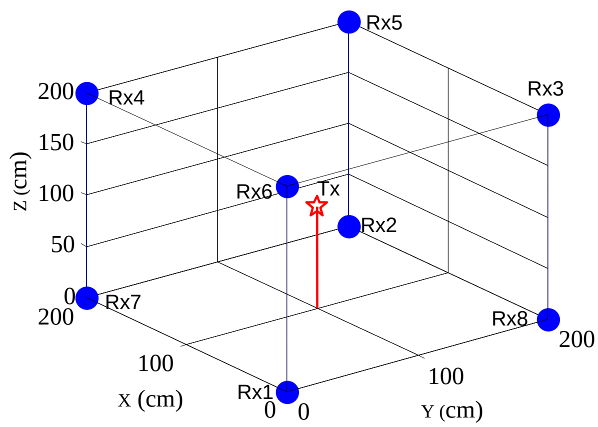


Figure 4.1: Receiver geometry configuration.

Table 4.1: Optimum GDOP versus the number of receivers.

| Receiver number | 4 | 5 | 6 | 7 | 8 |
|---|---|---|---|---|---|
| GDOP | 1.5 | 1.403 | 1.299 | 1.186 | 1.061 |

It is well known that every function can be approximated by a polynomial. From the simulation results, a quadratic function is used to derive the analytical relationship between the GDOP and the number of receivers:

$$\text{GDOP}(N) = aN^2 + bN + c, \;\; N = 4, \cdots, 8. \tag{4.7}$$

Substituting the simulation result into Eq. (4.7), we have

$$\mathbf{y} = \mathbf{A} \times \boldsymbol{\theta} \tag{4.8}$$

where $\mathbf{y} = [\text{GDOP}(4), \cdots, \text{GDOP}(8)]^T$, $\boldsymbol{\theta} = [a, b, c]^T$, and

$$\mathbf{A} = \begin{bmatrix} 4^2 & 4 & 1 \\ 5^2 & 5 & 1 \\ 6^2 & 6 & 1 \\ 7^2 & 7 & 1 \\ 8^2 & 8 & 1 \end{bmatrix}. \tag{4.9}$$

Using the least-square method, we can calculate $\boldsymbol{\theta}$ as

$$\boldsymbol{\theta} = (\mathbf{A}^T\mathbf{A})^{-1}\mathbf{A}^T\mathbf{y} = [-0.005, -0.053, 1.788]^T. \tag{4.10}$$

The reconstructed function of the optimum GDOP is

$$\text{GDOP}(N) = -0.005N^2 - 0.053N + 1.788. \tag{4.11}$$

### 4.4.2 Average GDOP Simulation

In Sec. 4.4.1, we have analyzed the GDOP for the special case when the transmitter is at the center. However, in real applications, the transmitter could be placed anywhere inside the area. Therefore, it is more meaningful to calculate the average GDOP for different transmitter positions. In this simulation, 729 transmitter positions in a grid as shown in Fig. 4.2 are assessed, and the average GDOP of these transmitters is calculated. The TDOA estimation error model is the same as the previous simulation. The function between the average GDOP and the number of receivers is

$$\mathrm{GDOP}_{ave}(N) = -0.0001N^2 - 0.1598N + 2.4271. \tag{4.12}$$

Comparison of the optimum GDOP and the average GDOP with their reconstructed functions is given in Fig. 4.3. From Fig. 4.3, we observe that the GDOPs decrease linearly as the number of receivers increases and the reconstructed GDOPs agree with the simulated GDOPs, which validates the accuracy of the reconstructed functions.

## 4.5 PEB Simulation with Different Combinations of Distance Measurement Error

Multipath overlap is one of the major technical challenges that must be overcome for designing a high-precision localization system [42]. In this section, we evaluate how the PEB varies with the signal bandwidth and the number of re-

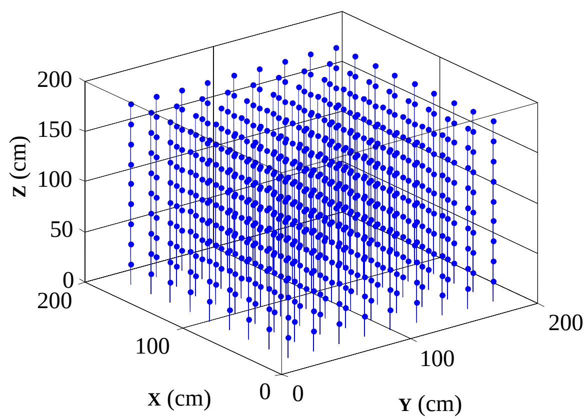


Figure 4.2: Position of the transmitters for evaluating the average GDOP.

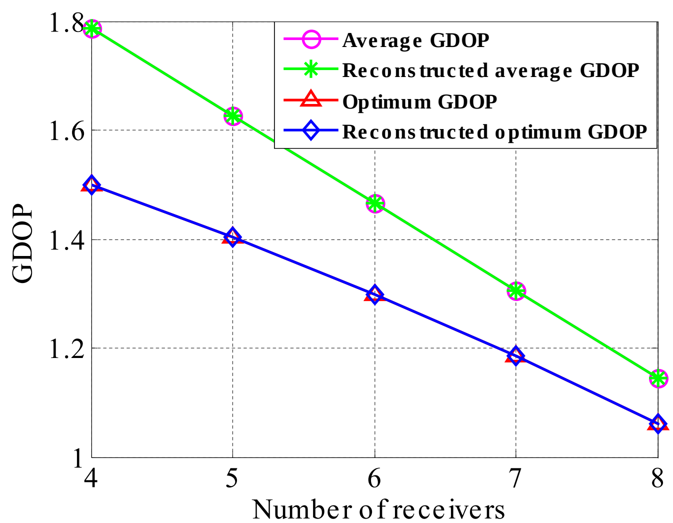


Figure 4.3: GDOP versus the number of receivers.

ceivers in the presence of multipath overlap. This requires a model of distance measurement error (DME) caused by multipath overlap. One such model is given in [47], where the DME is modeled as having a Gaussian distribution that is related to the signal bandwidth and the distance between the transmitter and the receiver as:

$$\text{DME} = \begin{cases} \ln(1+d)G(2, 13.6), & Bw = 1 \text{ GHz} \\ \ln(1+d)G(2, 5.2), & Bw = 2 \text{ GHz} \\ \ln(1+d)G(2, 4.5), & Bw = 3 \text{ GHz}. \end{cases}$$

In the analysis, $d = 2$ m is chosen for the DME modeling since the area in which the simulation is conducted is about $2 \times 2 \times 2$ m$^3$. We consider the situation when only portions of the receivers have multipath overlap, called multipath overlap density here. For example, 25% overlap density means that 25% of receivers have multipath overlap DME. When multipath overlap is present for a particular receiver, the DME model given in [47] is used; otherwise the distance estimation error is assumed to be caused by a zero-mean Gaussian noise. The final PEB estimate for each case is obtained from 100 Monte-Carlo experiments.

The PEB of the transmitter at the center is shown in Fig. 4.4, Fig. 4.5 and Fig. 4.6, and the average PEB is shown in Fig. 4.7, Fig. 4.8 and Fig. 4.9. With the same signal bandwidth and multipath overlap density, the PEB of the transmitter at the center is lower than the average PEB. In addition, the PEB decreases as the signal bandwidth increases.

These results are very useful for designing practical localization systems. For example, in order to design a centimeter-level localization system, one can

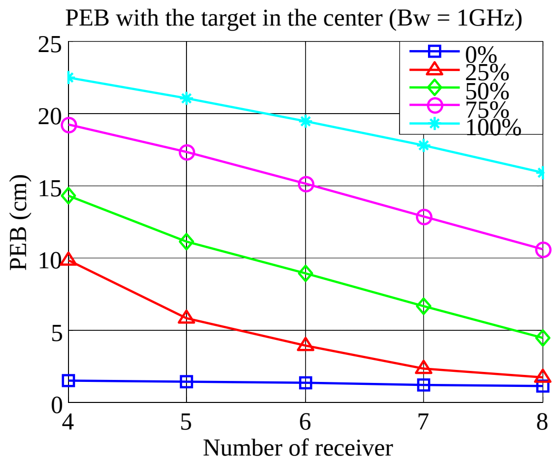


Figure 4.4: PEB of the center transmitter vs the number of receivers ($Bw$=1 GHz).

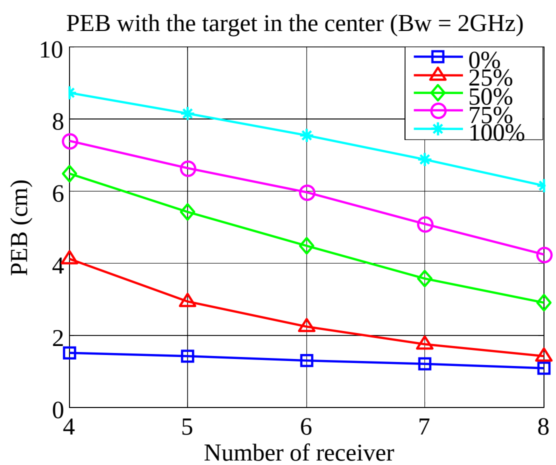


Figure 4.5: PEB of the center transmitter vs the number of receivers ($Bw$=2 GHz).

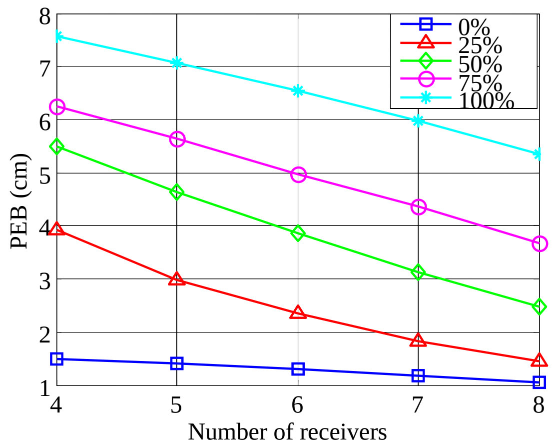


Figure 4.6: PEB of the center transmitter vs the number of receivers ($Bw$=3 GHz).

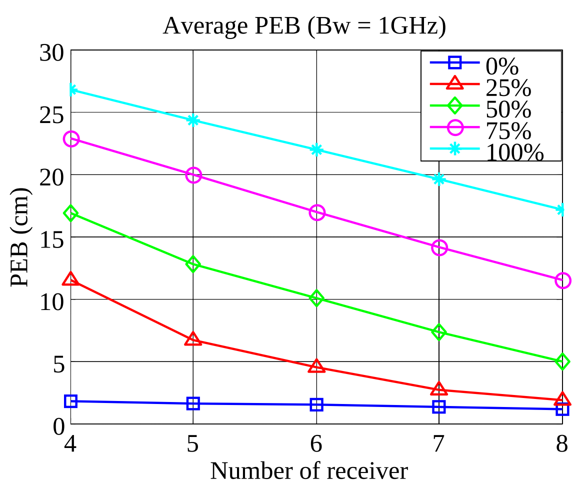


Figure 4.7: Average PEB vs the number of receivers ($Bw$=1 GHz).

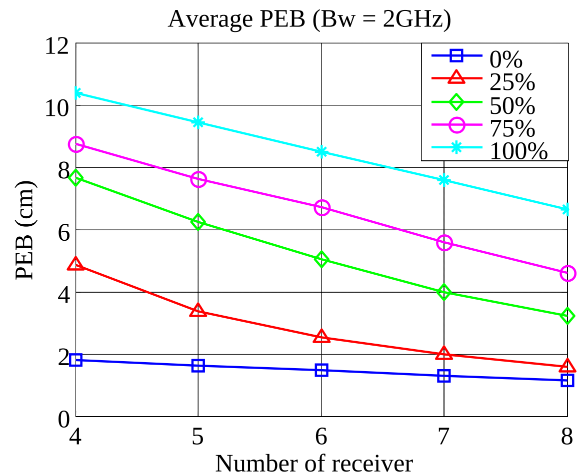


Figure 4.8: Average PEB vs the number of receivers ($Bw$=2 GHz).

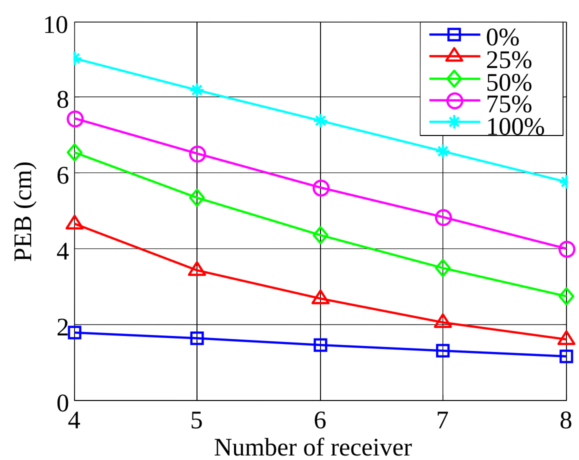


Figure 4.9: PEB of the center transmitter vs the number of receivers ($Bw$=3 GHz).

determine the required signal bandwidth and the number of receivers by using the results in this paper.

## 4.6 Conclusion

The GDOP of TDOA localization is investigated for different numbers of receivers assuming a near-optimum receiver geometric configuration. The analytical relationship between the GDOP and the number of receivers is derived. By using the UWB indoor distance error model, the PEB is simulated with different signal bandwidths, number of receivers, and multipath overlap densities. These results provide a useful guidance for designing real localization systems in terms of the required signal bandwidth and the number of receivers.

# Chapter 5 – UWB TDOA Wireless Localization System

## 5.1 Introduction

A centimeter-accurate UWB localization system for tracking miniature mechanical parts in airplane wheel-well is introduced in [12]. TDOA methods are applied in this system and a four-channel data-acquisition unit (DAU) is used to sample the received signals. Since all channels of the DAU share a common clock, no receiver synchronization is required. The main advantage of this system is the high localization accuracy.

For most applications, systems that do not require wires to connect the receivers are attractive. One major challenge of implementing a wireless localization system is the synchronization between the receivers. Picosecond synchronization accuracy is needed to achieve centimeter localization accuracy. The need of a high synchronization accuracy makes the system design very challenging. To the best of our knowledge, there is no wireless localization system with centimeter accuracy reported either in the commercial products or in the literature reports [1, 5–11, 57]. In [57], a localization system with an accuracy of 22 cm using UWB radio is presented.

In this chapter, we present a wireless prototype localization system with centimeter-accuracy using the TDOA method. The basic concept of this system will be introduced and a two-step synchronization method is proposed. One experiment is conducted in a laboratory environment, which shows the potential of this system to achieve a centimeter accuracy in an indoor environment. The limitation of the system as well as future work will be discussed.

## 5.2 Wireless Localization System

The wireless localization system is shown in Fig. 5.1. This system consists of a UWB target transmitter whose location to be estimated, a synchronization transmitter (sync node), four receivers and a main signal processor (computer). The target transmitter and the sync node both generate a UWB pulse with bandwidth about 1 GHz and the center frequency around 4 GHz. In the receiver, a ADC08D1500DEV Development board [55] made by National Semiconductor is used to handle data acquisition, which includes an ADC with a sampling rate of 3 Gsps and an FPGA.

The received signal goes through a square device and a low pass filter, to be down converted to the baseband. The bandwidth of the transmitted signal does not exceed 1.5 GHz so it can be sampled unambiguously by the ADC with a sampling rate of 3 Gsps. All the transmitters, receivers and computer have WLAN interfaces, which enable efficient data package exchange.

## 5.3 Synchronization

Since the four receivers do not share a common clock or trigger signal, synchronization is required for TDOA estimation. The basic concept of the synchronization method is summarized as follows [56]:

1. The target transmitter sends out a signal through WLAN to the sync node

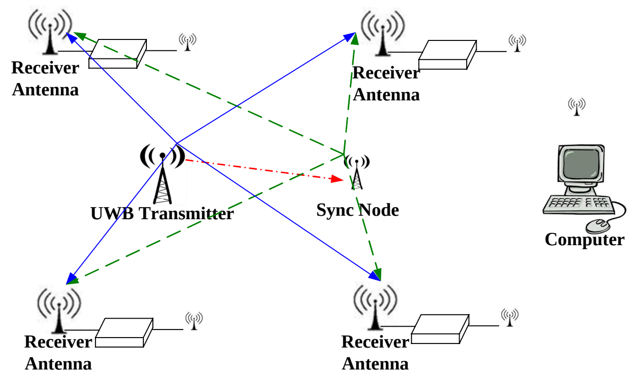


Figure 5.1: Wireless Localization System.

and the computer to start the synchronization process;

2. After receiving the synchronization requirement, the sync node starts to transmit a UWB signal to all four receivers;

3. The received signals are converted to the baseband through a receiver front-end board, and are then sampled by the ADCs;

4. A portion of the sampled signal is stored in the ADC buffer and sent to the computer via WLAN;

5. TOA based on the receivers local clocks are measured for all the four received signals. Since the sync node and the four receivers are at fixed locations, the distances between the receivers to the sync node are known, thus the clock offset of the four receivers can be calculated;

6. After synchronizing all the four receivers, the computer will send out a

message to the target transmitter to start transmitting UWB signals for localizations.

The mathematical representation of the synchronization process is given by Eq. (5.1) and Eq. (5.2):

$$\hat{t}_i = t_o + t_{pi} + T_{si} + e_i, i = 1, \cdots, N \tag{5.1}$$

where $\hat{t}_i$ is the TOA estimate of the synchronization signal at the $i$th receiver, $t_o$ is the time that the signal starts to transmit at the sync node, $t_{pi}$ is the signal traveling time from the sync node to the $i$th receiver, $T_{si}$ is the initial sampling time at the $i$th receiver, $e_i$ is the TOA estimation error caused by noise, multipath interference, etc. The synchronization of the receivers is to find out the time difference between the initial start sampling time of each receiver.

Since the positions of the sync node and the receivers are fixed, and only the LOS environment is considered, the distances between the sync node to all the receivers are known; thus $t_{pi}$ can be calculated. Without loss of generality, the first receiver is used as the reference node and the time offset can be estimated as

$$\begin{aligned}\hat{t}_{off}(i,1) &= \hat{t}_i - t_{pi} - \hat{t}_1 + t_{p1} \\ &= t_o + T_{si} + e_i - t_o - T_{s1} - e_1 \\ &= T_{si} - T_{s1} + e_i - e_1 \\ &= t_{off}(i,1) + e_i - e_1,\ i = 2, \cdots, N\end{aligned} \tag{5.2}$$

where $\hat{t}_{off}(i,1)$ is the clock offset estimate between the 1st and the ith receiver. Using (5.2), $\hat{t}_{off}(i,1)$ between the $i$th receiver and the 1st receiver can be calculated. The synchronization accuracy is closely related to the TOA estimation accuracy. Since UWB signal has been proved to have high range estimation accuracy, it produces a high synchronization accuracy [12].

Because of the clock drift, it is impossible to synchronize the clock once and maintain the synchronization for a long time. For example, if the clock accuracy is 1 part per billion, the clock drift after 1 day could be 84.6 us. This error is not tolerable for a high precision localization system and the synchronization process needs to repeat every few seconds.

### 5.3.1 Coarse Synchronization

In addition to the clock drift, another factor that needs to be considered is the conflict between the high sampling rate and the limited buffer size of the ADC and the data transmission speed from the FPGA to the computer. Although the ADC is able to sample the data in real time, only a portion of the data can be saved and transfered to the computer while other samples will be dumped and ignored. To calculate the time offset of the receiver clocks, we need to ensure that all receivers capture the same signal transmitted at the same time and from the same position, which is *coarse synchronization*. Fig. 5.2 shows the data saved in different receivers before and after *coarse synchronization* [54, 56]. After coarse synchronization, all the data is saved almost at the same time for different receivers.

The problem needs to solve is how to trigger different receivers to save the data at approximately the same time. A straightforward method is to use a common signal to trigger the receivers to start sample and save the data. This

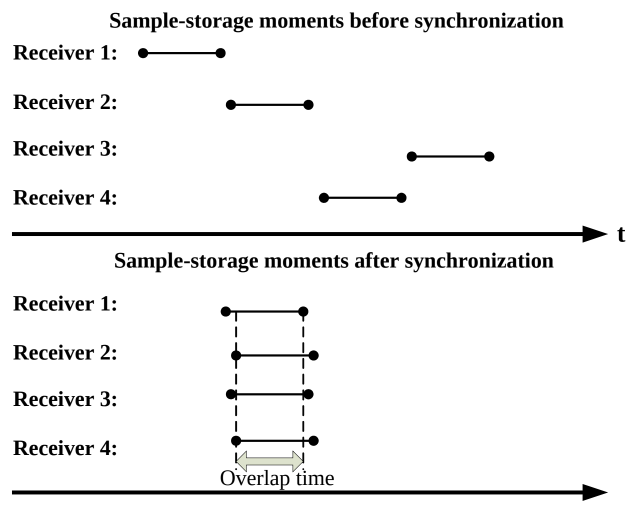


Figure 5.2: Necessity of coarse synchronization.

can be achieved by using the signal sent from the sync node. After the receivers are coarsely synchronized, we can control each receiver to save the data after every 100 ms within 5 seconds before the next synchronization is performed. The time interval for the data storage is called *time-window* in the rest of the thesis.

This method is simple but it brings in another problem regarding how to define the *time-window* through different receivers as they have slightly different clock speeds. To solve this new problem, instead of sending a single pulse, the sync node will send a certain number of pulses, which have to be counted by the FPGA in each receiver. While the FPGA counts the pulses, it also counts its own clock cycles. After a certain amount of pulses, all receivers stop counting their clock cycles. Since it takes them the same amount of time to count the pulses, all receivers now have a unique counting value that corresponds to the *time-window*. Fig. 5.3 shows the concept and the resulting counting in all receivers.

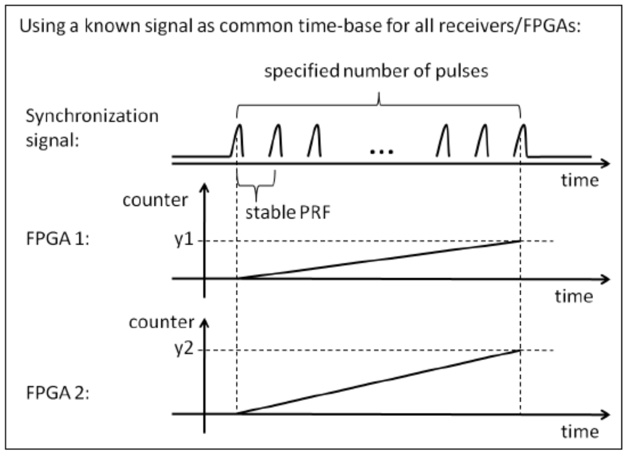


Figure 5.3: Synchronized time windows.

The *coarse synchronization* can synchronize the received data to a level of the FPGA clock speed that is $\frac{1}{16}$ times of the ADC sampling rate. Therefore, the accuracy of the *coarse synchronization* is within 5.3 ns. The pulse repetition rate for the synchronization pulse is about 100 ns, so the *coarse synchronization* can guarantee that all receivers capture the same signal transmitted at the same time and from the same position.

### 5.3.2 Fine Synchronization

With the roughly synchronized trigger system, each receiver saves samples in its buffer at approximately the same time. These samples will be sent to the computer via a reliable WLAN interface for fine synchronization. Fig. 5.4

illustrates the concept of fine synchronization .

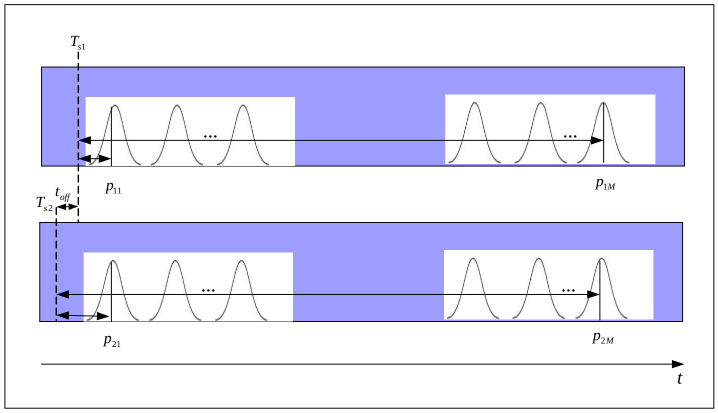


Figure 5.4: Illustration of fine synchronization: white boxes indicate the signal that have been captured by receivers and have been transfered to the computer; $p_{11}$ and $p_{21}$ denote the number of samples where the peak is detected for the first pulse at receiver 1 and 2; $p_{1M}$ and $p_{2M}$ denote the number of samples where the peak was detected for the M th pulse at receiver 1 and receiver 2; and $T_{s1}$ and $T_{s2}$ denote the start sampling time at receiver 1 and receiver 2.

The TOA estimation for the first pulse at receiver 1 and receiver 2 are

$$\begin{aligned} \hat{t}_{11} &= p_{11}/f_{s1} = t_{11} + e_{11} \\ \hat{t}_{21} &= p_{21}/f_{s2} = t_{21} + e_{21} \end{aligned} \tag{5.3}$$

where $e_{11}$ and $e_{21}$ are the TOA estimation errors caused by the noise and multipath interference, $t_{11}$ and $t_{21}$ are the actual TOAs of the first pulse at the two receivers.

Assume the signal processing time from the sync node to the two receivers are $t_{p1}$ and $t_{p2}$. Since the location of the sync node and the receivers are fixed, $t_{p1}$ and $t_{p2}$ are known. The $\hat{t}_{off}(2,1)$ between the 1st receiver and the second receiver can be estimated using (5.2) as

$$\begin{aligned}\hat{t}_{off}(2,1) &= \hat{t}_{21} - t_{p2} - \hat{t}_{11} + t_{p1} \\ &= \frac{p_{21}}{f_{s2}} - \frac{p_{11}}{f_{s1}} + t_{p1} - t_{p2} \\ &= t_{off}(2,1) + e_{21} - e_{11}.\end{aligned} \tag{5.4}$$

In (5.4), it is observed that the synchronization accuracy is closely related to the TOA estimation accuracy so it is very important to achieve a good TOA estimation accuracy. In addition to a high precision TOA estimation algorithm [12], we also need to carefully place the sync node and receivers to ensure LOS propagation.

Besides the TOA error, the sampling rate also needs to be carefully considered. All the ADCs have sampling rate around 3 Gsps. However, different hardwares have different performance. From our measurement, we found that the sampling rates for different receivers are not identical [56]. Moreover, the sampling rate slightly changes as the time goes by. If the clock difference between the two receivers are not compensated, large error will be brought to the TDOA estimation. For example, assume $f_{s1} = 3 \times 10^9$ Hz and $f_{s2} = 3.0000001 \times 10^9$ Hz with a difference of 100 Hz. If the difference is unknown, it can bring a bias of $1 - f_{s1}/f_{s2} = 33.33$ ns on TDOA estimation between these two receivers after running for 1 second. This error is huge for the high precision localization system and cannot be ignored. In order to reduce the effect of sampling rate on the synchronization, one new method is presented to estimate the difference between the different sampling rates. This new method is based on the fact that the clock offset for all the receivers are fixed.

Using receiver 1 and receiver 2 as an example, $T_{s2} - T_{s1}$ is fixed in each synchronization cycle. Therefore, we can use more than one pulse transmitted from the sync node to calculate $t_{off}(2,1)$. For example, we can use the 1st pulse and the Mth pulse to jointly estimate $t_{off}(2,1)$. To simplify this problem we assume that the distance between the sync node and the two receivers are the same, that is $t_{p1} = t_{p2}$. According to (5.4), we have

$$\begin{aligned} t_{off}(2,1) &= (T_{s2} - T_{s1}) \\ \frac{p_{11}}{f_{s1}} + e_{11} - \frac{p_{21}}{f_{s2}} - e_{21} &= \frac{p_{1M}}{f_{s1}} + e_{1M} - \frac{p_{2M}}{f_{s2}} - e_{2M} \\ f_{s2} &= \frac{p_{2M} - p_{21}}{p_{1M} - p_{11} + (e_{1M} - e_{2M} + e_{21} - e_{11})f_{s1}} f_{s1} \\ \hat{f}_{s2} &= \frac{p_{2M} - p_{21}}{p_{1M} - p_{11}} f_{s1} \end{aligned} \tag{5.5}$$

where $e_{11}, e_{21}, e_{1M}$ and $e_{2M}$ are the TOA estimation errors for the first pulse and the Mth pulse at receiver 1 and receive 2, respectively, $\hat{f}_{s2}$ is the estimate of $f_{s2}$. Here we set $f_{s1}$ as 3 Gsps, the difference between $f_{s2}$ and $f_{s1}$ can be estimated.

The estimation accuracy of $f_{s2}$ is a function of the TOA estimation errors $(e_{1M} - e_{2M} + e_{21} - e_{11})f_{s1}$ and the distance between the 1st and the Mth pulse $p_{1M} - p_{11}$. Since the TOA estimation error is inevitable, we can increase $p_{1M} - p_{11}$ to reduce the effect of the TOA estimation error on the sampling rate estimation. In addition, the small error on the sampling rate estimation will accumulate as time increases. Therefore, we need to repeat the synchronization as often as possible.

After the fine synchronization is complete, the target transmitter starts to transmit UWB signals to all the receivers. The TDOA between the target transmitter to all the receivers can be estimated, and the position of the target transmitter can be determined. The algorithms used for the TDOA and position estimation in the wireless system are the same as the one used in the wire system discussed in Chapter 3; thus the details will not be repeated in this chapter.

## 5.4 Experiment

In order to test the achievable accuracy of the wireless localization prototype system, an experiment is constructed and tested in a laboratory environment.

### 5.4.1 Experiment Setup

The experiment setup is shown in Fig. 5.5. This system consists of a computer, a UWB target transmitter, a sync node and four receivers (the minimum number of receivers required for 3-D positioning using TDOA method). The target transmitter and sync node are controlled by the computer via a wireless link. The signals from the receivers are transmitted to the computer wirelessly (802.11). The computer runs the software for localization, synchronization of the receivers, and control of the whole network. The prototype receiver is shown in Fig. 5.6 [54].

The positions of the receivers and sync node are fixed and their coordinates are measured with a measuring tape. The sync node is placed around the center

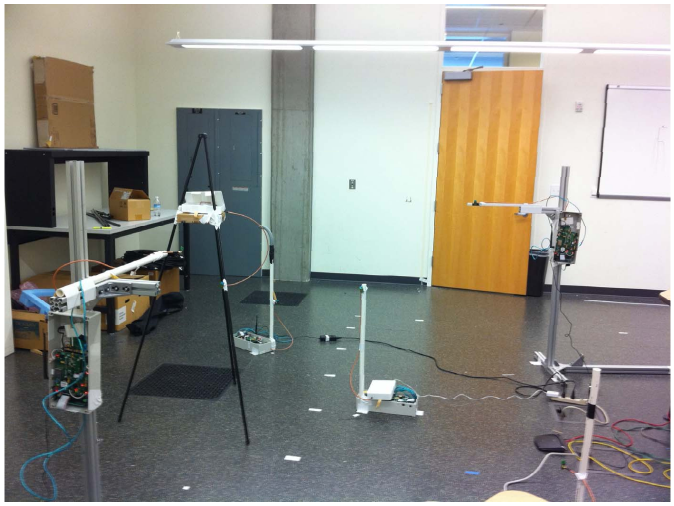

Figure 5.5: Experiment setup.

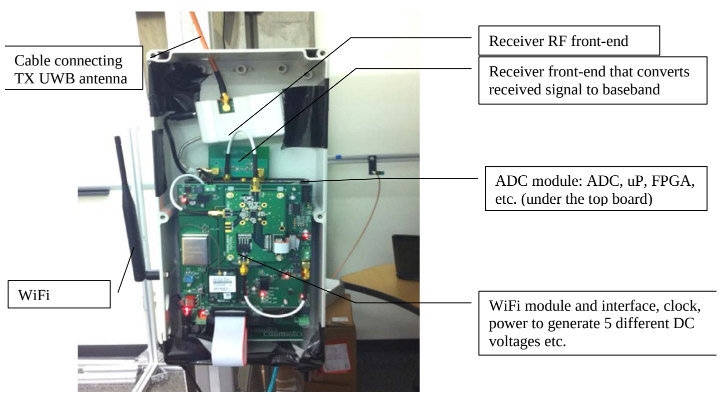


Figure 5.6: The prototype receiver.

of the configuration, and distances between the sync node to all the receivers are measured with a laser range finder. The system configuration is summarized as follows:

**1)** A target transmitter, a sync node and four receivers;

**2)** The sync node starts to transmit the UWB signal to synchronize all receivers;

**3)** After all receivers are synchronized, the sync node is set to be idle and the transmitter starts to transmit the UWB signal for localization;

**4)** The synchronization and localization signals are sampled by the four ADC boards and the sampled data is sent through Wi-Fi to the computer, where the localization algorithm runs in Matlab;

**5)** Six transmitter positions are chosen within the area confined by the receivers;

**6)** Twenty readings at each position are taken and the mean value of the 3-D position estimate is recorded.

The coordinates of the receivers, sync node and the six positions of the transmitters are shown in Fig. 5.7 and Table 5.1.

### 5.4.2 Experiment Result

Twenty readings are taken for each of the measured positions and the average estimation error for $(x, y, z)$-coordinates are calculated for each position. The estimation errors between the tape-measured and the radio-measured positions are given in Table 5.2, where $p_1$ to $p_6$ represent the six positions of the transmitter.

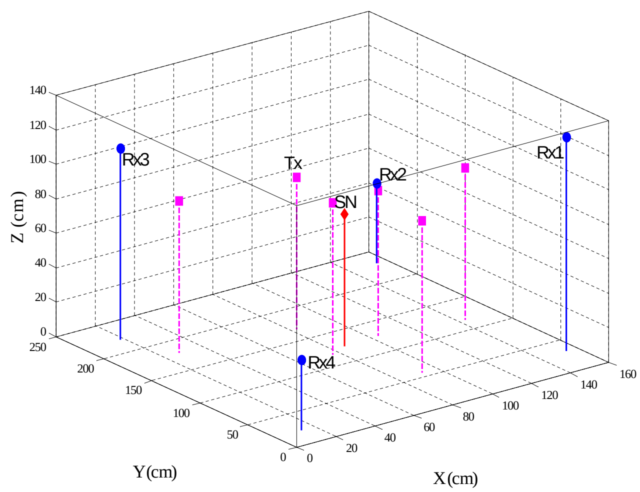


Figure 5.7: The position of the transmitter, receivers and sync node.

The experiment result shows that all the errors for x, y, and z coordinates are less than 5 cm. There are several factors that might affect the final localization accuracy:

1) Inaccurate receiver coordinates measured by the measuring tape;

2) Inaccurate distances measurement between the sync node and the receivers;

3) Synchronization error caused by multipath and noise;

4) Localization error caused by the synchronization error, multipath and noise effects;

5) Inaccurate transmitter coordinates measured by the measuring tape.

To the best of our knowledge, this system is the first to achieve an accuracy

Table 5.1: Tape-measured coordinates of the receivers, sync node and transmitters.

| | $x(cm)$ | $y(cm)$ | $z(cm)$ |
|---|---|---|---|
| Receiver 1 | 155 | 34.2 | 123.8 |
| Receiver 2 | 154.8 | 231.6 | 46 |
| Receiver 3 | 18.9 | 221.8 | 111.1 |
| Receiver 4 | 13.8 | 23 | 40.8 |
| Sync Node | 86.3 | 125.9 | 76.4 |
| $p_1$ | 105 | 128.5 | 87.6 |
| $p_2$ | 143.8 | 117 | 87.6 |
| $p_3$ | 83 | 168.5 | 87.6 |
| $p_4$ | 93 | 58.1 | 87.6 |
| $p_5$ | 28.7 | 181 | 87.6 |
| $p_6$ | 76.8 | 118.7 | 87.6 |

Table 5.2: Average estimation error for $(x, y, z)$-coordinates of the six positions.

| | $E_x(cm)$ | $E_y(cm)$ | $E_z(cm)$ |
|---|---|---|---|
| $p_1$ | -3.75 | 0.92 | 0.74 |
| $p_2$ | -0.33 | -0.01 | -4.17 |
| $p_3$ | -0.08 | 1.16 | 5.9 |
| $p_4$ | 0.09 | 4.06 | -0.2 |
| $p_5$ | -1.04 | 4.73 | 3.23 |
| $p_6$ | -3.83 | -1.75 | 2.44 |

within a few centimeters with all wireless receivers. The systems with the closest performance to ours are reported in two papers [57] and [58], with about 22 cm and 36 cm accuracies, respectively, for 2-D localization ((x,y)-coordinates only).

The theoretical analysis and experiment result shows that this wireless localization system has the potential to achieve centimeter accuracy. In order to increase the localization accuracy, further refinements and improvements are needed:

1) Adding more receivers;

2) Averaging more independent estimates to eliminate the effects of random noise and random synchronization errors;

3) Better receiver front-end design, and better transmit and receive antenna design;

4) Higher signaling bandwidth; however, this will result in challenges in designing RF components such as ADC, filters, amplifiers, and antennas.

## 5.5 Conclusion

We have introduced a wireless localization system prototype with centimeter accuracy using TDOA method. The two-step synchronization method has been analyzed and the factors affecting the synchronization and localization accuracy have also been discussed. An experiment is conducted in the laboratory environment and it is proved that the wireless localization system has the potential to achieve a centimeter accuracy.

Even though wireless localization with centimeter accuracy is feasible, it is still very challenging to implement the system. The requirement for high precision wireless synchronization makes the system design and setup very difficult and complicated. Many factors such as the TOA estimation error, different clock speeds, imperfect receiver front-end design, etc. all can affect the synchronization accuracy and make the system unstable. In addition, executing synchronization and message exchange between the target transmitter and the sync node make the localization process very slow.

These limitations of the high precision wireless localization system might prevent it from being widely used. A simpler system without wireless synchronization will be a better solution for many applications.

# Chapter 6 – UWB TOA Localization System with Collocated Receivers

## 6.1 Introduction

Most of the UWB localization systems reported so far use multiple distributed receivers with the transmitter located inside the geometry. Recently, a 3-D UWB localization system with decimeter accuracy using a single receiver unit is reported in [48]. TOA and AOA techniques are used in this system. Compared with other UWB localization systems, the single receiver unit localization system has several advantages such as the simple system design and easy system setup.

We introduce and analyze an UWB 3-D localization system that employs a single cluster of receivers placed in proximity (e.g., on a 2-D plane within a few decimeters) in this chapter. This system employs TOA technique, and since receivers are placed in proximity, the system does not need to synchronize the receivers wireless, resolving one of the major technical challenges for conventional TOA schemes with distributed receivers. We analyze optimum receiver placement in the sense of minimum estimation variance defined by the CRLB derived under the AWGN model, and derive GDOP as a function of the number of receivers and the distance between the transmitter and the receiver unit. We also construct a hardware and software prototype that works in the 3.1 – 5.1 GHz range, and test it in a laboratory environment. We will show, with experimental results, that with four receivers placed within a square of side length of 8.5 decimeters, the maximum error (distance between estimated and actual positions) for sources that within 10 meters from the receiver unit is about 8 decimeter.

## 6.2 System Model

Consider a system with one small receiver unit that houses all receivers and a nearby transmitter, whose location in a 3-D space relative to that of the receivers is to be determined. The coordinates of all $M$ receivers expressed as $\mathbf{Q} = [\mathbf{q}_1, \mathbf{q}_2, \cdots, \mathbf{q}_M]$ are known, where $\mathbf{q}_i = [x_i, y_i, z_i]^T$ represents the $\{x, y, z\}$-coordinates of the $i$th receiver. The unknown coordinate $\mathbf{p} = [x, y, z]^T$ of the target transmitter is to be estimated. Since the receivers are located in proximity, they are synchronized via wire connection. With TOA, the transmitter still needs to be synchronized with the receiver unit, but this is much easier to achieve than synchronizing many distributed receivers and the transmitter wirelessly.

Without loss of generality, the first receiver is designated as the master node. The master node sends a ranging request to the transmitter and records a time stamp $t_0$ when the ranging request departs. Upon receiving the ranging request, the transmitter transmits an UWB signal. Assuming that the signal processing time in the transmitter is known and fixed, the TOA of the signal from the transmitter to all receivers could be calculated. The estimated distance $\hat{d}_i$

between the transmitter and the $i$th receiver is modeled as

$$\begin{aligned}\hat{d}_i &= d_i + b_i + n_i \\ &= \|\mathbf{p} - \mathbf{q}_i\| + b_i + n_i, i = 1, \cdots, M\end{aligned} \tag{6.1}$$

where $d_i = \|\mathbf{p} - \mathbf{q}_i\|$ is the actual distance between the $i$th receiver and the transmitter ($\|.\|$ denotes $\ell_2$ norm), $b_i$ is a positive bias caused by NLOS propagation and $n_i$ is a Gaussian random variable with zero mean and variance $\sigma^2$. Only the LOS case is considered; thus $b_i = 0$.

TOA 3-D localization requires at least four range estimates to obtain an unambiguous position estimate. However, if the receiver unit is placed in the same plane and the transmitter is always located on one side of this plane, then three range estimates are sufficient. An example of this system is shown in Fig. 6.1, where all the receivers are placed in the same plane. For most indoor applications, these receiver could be placed along a wall or the ceiling, as illustrated in Fig. 6.1.

## 6.3 Optimum Receiver Geometry

Two main questions about the localization system with collocated receivers need to be answered: (a) Given a confined area where receivers can be placed in, how should the receivers be arranged for best performance? (b) Given a certain receiver geometry and distance between a transmitter and the receiver unit, what localization accuracy is achievable?

The difficulty in answering question (a) lies in the fact that an optimum geometric receiver configuration for all target locations does not exist. For indoor

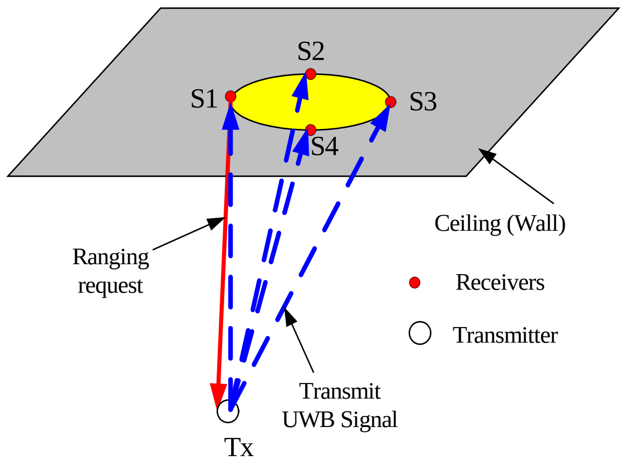


Figure 6.1: Illustration of the system configuration.

applications, however, the receiver unit could be mounted on a wall or a ceiling of a room, with its center facing the center of items/activities whose locations are to be tracked. In this case, an optimum receiver geometric configuration is possible for the transmitter located at the center of activity. We will take this approach in deriving the optimum receiver geometry in this section, and the optimality is in the sense of minimum estimation variance determined from the CRLB. Given the optimum receiver geometric configuration for a target located at the center of activity, a lower bound on the position error could be derived analytically; for targets at other locations, simulation could be resorted to obtain the localization accuracy.

### 6.3.1 Cramér-Rao Lower Bound for TOA Localization

CRLB is a lower bound for the variance of an unbiased estimator. It is often used as a benchmark for estimation performance. Let the $M$ independent range estimates obtained by the $M$ receivers be $\hat{\mathbf{d}} = [\hat{d}_1, \hat{d}_2, \cdots, \hat{d}_M]$ with corresponding mean values $\mathbf{d} = [d_1, d_2, \cdots, d_M]$ and the same variance $\sigma^2$. As commonly accepted, the range estimation error is modeled as a Gaussian random variable. The CRLB is written as [27]

$$\mathbf{J}^{-1} = \sigma^2(\mathbf{G}\mathbf{G}^T)^{-1} \tag{6.2}$$

where $\mathbf{J}$ is the Fisher information matrix (FIM) and $\mathbf{G} = [\mathbf{g}_1, \mathbf{g}_2, ..., \mathbf{g}_M]$ with

$$\mathbf{g}_i = \frac{\mathbf{p} - \mathbf{q}_i}{\|\mathbf{p} - \mathbf{q}_i\|}. \tag{6.3}$$

One of the criteria to optimize the receiver geometry is to minimize the trace of the CRLB, which can be written as

$$\min_{\boldsymbol{g}_i} f_{\mathrm{CRLB}} = \mathtt{tr}\left[\mathbf{J}^{-1}\right] = \sigma^2 \mathtt{tr}\left[(\mathbf{G}\mathbf{G}^T)^{-1}\right] \tag{6.4}$$

where $\mathtt{tr}(\cdot)$ denotes the trace.

### 6.3.2 Optimization of Receiver Geometric Configuration

The system configuration is as follows.

1) The receivers must lie on or inside a circle with a radius of $L$, and the

center of the circle is designated as the origin.

2) The number of receivers is $M \geq 3$.

3) The transmitter is assumed to be located along a line that is perpendicular to the plane formed by the receivers and intersects with the plane at the origin.

Since the specific value of $\sigma^2$ do not affect the receiver geometry optimization, for simplicity, we let $\sigma = 1$ in the derivation.

With this system configuration, the transmitter position is expressed as $p = [0, 0, d]^T$, and the position of the $i$th receiver can be written as $\mathbf{q}_i = [l_i \cos\alpha_i, l_i \sin\alpha_i, 0]^T$, where $\alpha_i$ denotes the angle between the $x$-axis and the line formed by the position of the $i$th receiver and the origin and $l_i \leq L$.

$$\mathbf{J}=\begin{bmatrix} \sum_{i=1}^{M} \frac{l_i^2 \cos^2\alpha_i}{l_i^2+d^2} & \sum_{i=1}^{M} \frac{l_i^2 \cos\alpha_i \sin\alpha_i}{l_i^2+d^2} & \sum_{i=1}^{M} \frac{-dl_i \cos\alpha_i}{l_i^2+d^2} \\ \sum_{i=1}^{M} \frac{l_i^2 \cos\alpha_i \sin\alpha_i}{l_i^2+d^2} & \sum_{i=1}^{M} \frac{l_i^2 \sin^2\alpha_i}{l_i^2+d^2} & \sum_{i=1}^{M} \frac{-dl_i \sin\alpha_i}{l_i^2+d^2} \\ \sum_{i=1}^{M} \frac{-dl_i \cos\alpha_i}{l_i^2+d^2} & \sum_{i=1}^{M} \frac{-dl_i \sin\alpha_i}{l_i^2+d^2} & \sum_{i=1}^{M} \frac{d^2}{l_i^2+d^2} \end{bmatrix}. \tag{6.5}$$

We wish to minimize $\mathtt{tr}[\mathbf{J}^{-1}]$. When $d \neq 0$, $\mathbf{J}$ is a positive definite symmetric matrix, which has several useful properties [61] that we can exploit:

1) The diagonal entries $J_{i,i}$ are real and positive.

2) $\mathtt{tr}[\mathbf{J}] > 0$.

3) $|J_{i,j}| \leq \sqrt{J_{i,i}J_{j,j}} \leq \frac{1}{2}(J_{i,i} + J_{j,j})$.

The determinant of $\mathbf{J}$ is expressed as

$$|\mathbf{J}| = J_{1,1}(J_{2,2}J_{3,3} - J_{2,3}^2) - J_{1,2}^2 J_{3,3} - J_{1,3}^2 J_{2,2} + 2J_{1,2}J_{1,3}J_{2,3} \tag{6.6}$$

and the first diagonal element of the inverse matrix $\mathbf{J^{-1}}$, $\mathbf{J^{-1}_{(1,1)}}$, is expressed as

$$\mathbf{J^{-1}_{(1,1)}} = \frac{(J_{2,2}J_{3,3} - J_{2,3}^2)}{J_{1,1}(J_{2,2}J_{3,3}-J_{2,3}^2)-(J_{1,2}^2J_{3,3}+J_{1,3}^2J_{2,2}-2J_{1,2}J_{1,3}J_{2,3})}. \tag{6.7}$$

The second term of the denominator of $\mathbf{J^{-1}_{(1,1)}}$ is always greater than or equal to zero:

$$\begin{aligned} & J_{1,2}^2J_{3,3} + J_{1,3}^2J_{2,2} - 2J_{1,2}J_{1,3}J_{2,3} \\ & \geq J_{1,2}^2J_{3,3} + J_{1,3}^2J_{2,2} - |2J_{1,2}J_{1,3}J_{2,3}| \\ & \geq J_{1,2}^2J_{3,3} + J_{1,3}^2J_{2,2} - \left|2J_{1,2}J_{1,3}\sqrt{J_{2,2}J_{3,3}}\right| \\ & = \left(|J_{1,2}|\sqrt{J_{3,3}} - |J_{1,3}|\sqrt{J_{2,2}}\right)^2 \geq 0, \end{aligned} \tag{6.8}$$

where we have applied the property of a positive definite symmetric matrix, which results in $|J_{2,3}| \leq \sqrt{J_{2,2}J_{3,3}}$, in the second step. Therefore,

$$\mathbf{J^{-1}_{(1,1)}} \geq \frac{(J_{2,2}J_{3,3} - J_{2,3}^2)}{J_{1,1}(J_{2,2}J_{3,3} - J_{2,3}^2)} = \frac{1}{J_{1,1}}. \tag{6.9}$$

Similarly, we can prove that

$$\mathbf{J^{-1}_{(2,2)}} \geq \frac{1}{J_{2,2}}, \tag{6.10a}$$

$$\mathbf{J^{-1}_{(3,3)}} \geq \frac{1}{J_{3,3}}. \tag{6.10b}$$

From Eqs. (6.9) and (6.10), we conclude that $\mathtt{tr}[\mathbf{J}^{-1}]$ is minimized when $J_{i,j} = 0, i \neq j$, and

$$\mathbf{J} = \begin{bmatrix} \sum_{i=1}^{M} \frac{l_i^2 \cos^2 \alpha_i}{l_i^2+d^2} & 0 & 0 \\ 0 & \sum_{i=1}^{M} \frac{l_i^2 \sin^2 \alpha_i}{l_i^2+d^2} & 0 \\ 0 & 0 & \sum_{i=1}^{M} \frac{d^2}{l_i^2+d^2}. \end{bmatrix}. \tag{6.11}$$

The minimum of $\mathtt{tr}[\mathbf{J}^{-1}]$ is thus obtained as

$$\begin{aligned} \mathtt{tr}[\mathbf{J}^{-1}] &= \frac{1}{\sum_{i=1}^{M} \frac{l_i^2 \cos^2 \alpha_i}{l_i^2+d^2}} + \frac{1}{\sum_{i=1}^{M} \frac{l_i^2 \sin^2 \alpha_i}{l_i^2+d^2}} + \frac{1}{\sum_{i=1}^{M} \frac{d^2}{l_i^2+d^2}} \\ &= \frac{\sum_{i=1}^{M} \frac{l_i^2}{l_i^2+d^2}}{\frac{1}{4}(\sum_{i=1}^{M} \frac{l_i^2}{l_i^2+d^2})^2 - \frac{1}{4}(\sum_{i=1}^{M} \frac{l_i^2 \cos 2\alpha_i}{l_i^2+d^2})^2} + \frac{1}{\sum_{i=1}^{M} \frac{d^2}{l_i^2+d^2}} \\ &\geq \frac{4}{\sum_{i=1}^{M} \frac{l_i^2}{l_i^2+d^2}} + \frac{1}{\sum_{i=1}^{M} \frac{d^2}{l_i^2+d^2}} \end{aligned} \tag{6.12}$$

The equality holds when $\sum_{i=1}^{M} \frac{l_i^2 \cos 2\alpha_i}{l_i^2+d^2} = 0$.

In real applications, the distance between the transmitter and the receiver unit is usually much bigger than the size of the unit, that is $d >> L \geq l_i$. Therefore, we have $\frac{d^2}{l_i^2+d^2} \approx 1$, and (6.12) can be approximated as

$$
\begin{aligned}
\mathtt{tr}[\mathbf{J}^{-1}] &\geq \frac{4}{\sum_{i=1}^{M} \frac{l_i^2}{l_i^2+d^2}} + \frac{1}{\sum_{i=1}^{M} \frac{d^2}{l_i^2+d^2}} \\
&\approx \frac{4}{\sum_{i=1}^{M} \frac{l_i^2}{l_i^2+d^2}} + \frac{1}{M} \\
&= \frac{4}{\sum_{i=1}^{M} \frac{1}{1+(\frac{d}{l_i})^2}} + \frac{1}{M} \\
&\geq \frac{4}{\sum_{i=1}^{M} \frac{1}{1+(\frac{d}{L})^2}} + \frac{1}{M} \\
&= \frac{5+4(\frac{d}{L})^2}{M}.
\end{aligned} \tag{6.13}
$$

The last equality holds when $l_i = L$, for $i = 1, ..., M$. Therefore, by combining all the conditions for minimizing $\mathtt{tr}[\mathbf{J}^{-1}]$, it is easy to show that the sufficient conditions of the optimum receiver configurations are

$$l_i = L, i = 1, 2, ..., M \tag{6.14a}$$

$$\sum_{i=1}^{M} \sin 2\alpha_i = 0, \ \sum_{i=1}^{M} \cos 2\alpha_i = 0 \tag{6.14b}$$

$$\sum_{i=1}^{M} \sin \alpha_i = 0, \ \sum_{i=1}^{M} \cos \alpha_i = 0. \tag{6.14c}$$

Eq. (6.14a) shows that all receivers must be placed on the circle. We can further show that the UAA geometric configuration meets (6.14b) and (6.14c), and is the optimum receiver geometry.

A UAA is a configuration where the angle separations between any two adjacent receivers subtended at the origin are identical. With a UAA, the position of the $i$th receiver is written as

$$\alpha_i = \alpha_0 + \frac{2\pi}{M}(i-1), \ (i = 1, \cdots, M). \tag{6.15}$$

From the arithmetic progression [53], we have

$$\sum_{i=0}^{M} \sin(\phi + i\alpha) = \frac{\sin\frac{(M+1)\alpha}{2}\sin\left(\phi + \frac{M\alpha}{2}\right)}{\sin\left(\frac{\alpha}{2}\right)} \tag{6.16a}$$

$$\sum_{i=0}^{M} \cos(\phi + i\alpha) = \frac{\sin\frac{(M+1)\alpha}{2}\cos\left(\phi + \frac{M\alpha}{2}\right)}{\sin\left(\frac{\alpha}{2}\right)}. \tag{6.16b}$$

Therefore,

$$\sum_{i=1}^{M} \cos(2\alpha_i) = \frac{\sin(2\pi)\cos\left(2\alpha_0 + \frac{(M-1)2\pi}{M}\right)}{\sin(\frac{2\pi}{M})} = 0 \tag{6.17a}$$

$$\sum_{i=1}^{M} \sin(2\alpha_i) = \frac{\sin(2\pi)\sin\left(2\alpha_0 + \frac{(M-1)2\pi}{M}\right)}{\sin(\frac{2\pi}{M})} = 0. \tag{6.17b}$$

It is important to note that (6.17) is true only when $M \geq 3$, which is the minimum number of receivers required for this system. Thus, the remaining two of the sufficient conditions, (6.14b) and (6.14c), that ensure the system to achieve the minimum CRLB are satisfied with a UAA.

#### 6.3.2.1 When $d = 0$

The derivation above assumes that $d \neq 0$. For the special case when the transmitter is at the origin, that is, $d = 0$, the FIM is simplified as

$$\mathbf{J} = \begin{bmatrix} \sum_{i=1}^{M} \cos^2 \alpha_i & \sum_{i=1}^{M} \cos \alpha_i \sin \alpha_i \\ \sum_{i=1}^{M} \cos \alpha_i \sin \alpha_i & \sum_{i=1}^{M} \sin^2 \alpha_i \end{bmatrix}. \tag{6.18}$$

The trace of $\mathbf{J}^{-1}$ as a function of $l_i$ is expressed as

$$\mathtt{tr}[\mathbf{J}^{-1}] = \frac{4M}{M^2 - \left(\sum_{i=1}^{M} \cos 2\alpha_i\right)^2 - \left(\sum_{i=1}^{M} \sin 2\alpha_i\right)^2}, \tag{6.19}$$

which is minimized when

$$\sum_{i=1}^{M} \cos 2\alpha_i = 0 \tag{6.20a}$$

$$\sum_{i=1}^{M} \sin 2\alpha_i = 0. \tag{6.20b}$$

The minimum is obtained as

$$\mathtt{tr}[\mathbf{J}^{-1}] = \frac{4}{M}. \tag{6.21}$$

Therefore, the sufficient conditions to optimize the receiver geometry are (6.20). which, as expected, shows that a UAA would remain to be the optimum receiver geometry.

As discussed at the beginning of this section, an optimum receiver geometry for all transmitter positions does not exist, but in practice the receiver unit could be installed to face the center of the items/activities whose positions are to be tracked, and consequently the results derived are useful in the sense that the resulting receiver geometric configuration works best most of the times.

## 6.4 Position Error Bound

In this section we answer the second question posed at the beginning of Sec. 6.3. While it is difficult, if not impossible, to determine analytical localization accuracy as a function of a few system parameters, some tight bounds will be useful in practice. We will assume a UAA receiver geometric configuration as derived in the previous section.

### 6.4.1 When the Target is Located on a Line Perpendicular to the Receiver Plane

In this case, the coordinate of the transmitter is expressed as $\mathbf{p} = [0, 0, d]^T$ $(d > 0)$. The configuration is illustrated in Fig. 6.2.

When the optimum receiver geometry is used, the CRLB as a function of the distance $d$ and the number of receivers $M$ is written as

$$\mathbf{J^{-1}} = \sigma^2 \begin{bmatrix} \frac{2(L^2+d^2)}{ML^2} & 0 & 0 \\ 0 & \frac{2(L^2+d^2)}{ML^2} & 0 \\ 0 & 0 & \frac{L^2+d^2}{Md^2} \end{bmatrix}. \tag{6.22}$$

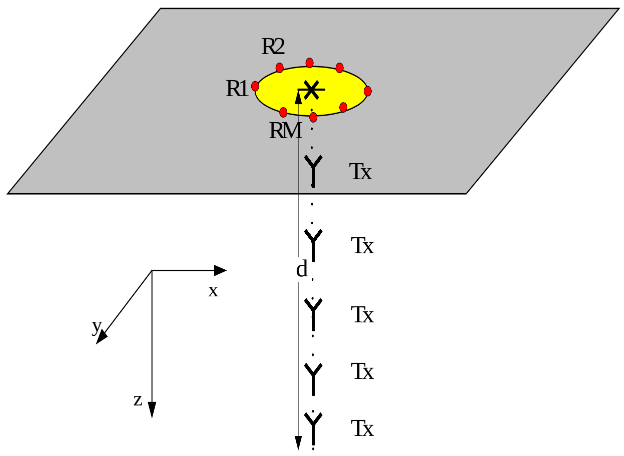


Figure 6.2: Receiver configuration for PEB derivation.

The PEB is thus expressed as

$$\mathrm{PEB}(\mathbf{d}) = \sqrt{\mathrm{tr}[\mathbf{J}^{-1}]} = \frac{\sigma}{L}\sqrt{\frac{4d^4 + 5d^2L^2 + L^4}{Md^2}}. \tag{6.23}$$

The PEB expression in (6.23) is a convex function of $d$ and the minimum PEB of PEB $= \sqrt{\frac{9}{M}}\sigma$ is reached when $d = \frac{\sqrt{2}L}{2}$. The PEB decreases as the number of receivers, $M$, by a factor of $1/\sqrt{M}$. The PEB versus the distance $d$ and the number of receivers $M$ will be calculated assuming the following parameters: the radius of the localization receiver unit is $L = 0.5$ m and the number of receivers, $M$, equals $4, 6$, and 8.

Range error models with pulsed UWB signals in indoor environments have been derived in [47, 62]; for LOS cases, it is shown that range errors can be modeled as a Gaussian random variable. With a signal bandwidth of 1 GHz, the standard deviation of the range error will not exceed 0.1 m [62]; further increase the bandwidth will result in even smaller errors. Also, in practice, many independent range measurements will be taken for one final estimate, like what we implemented in our experiment that will be described in Sec. 6.5. We have found that with a 1.5−2 GHz signal bandwidth and by implementing better algorithms [12] and by averaging 10 range estimates, the standard deviation of range estimation errors could be as small as 0.01 m. Therefore, we set $\sigma = 0.01$ m for the PEB calculation in the following examples.

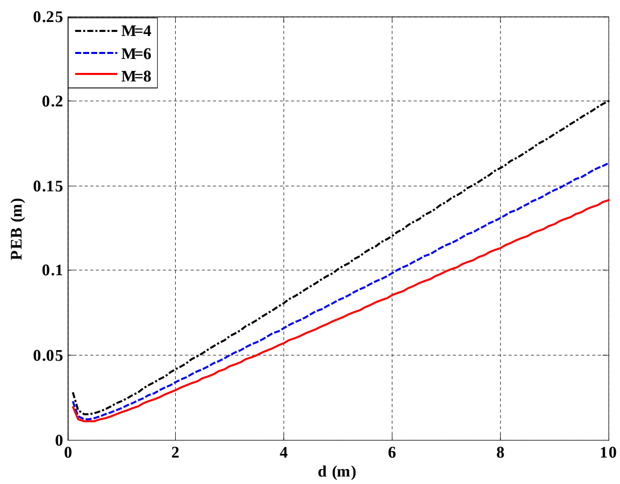


Figure 6.3: PEB vs the distance as a function of the number of receivers.

Fig. 6.3 shows how the PEB varies with the distance $d$ and the number of receivers $M$. Information such as what localization accuracy the system can achieve given a set of values of $M$ and $d$, or how many receivers and how big the receiver unit needs to be to achieve a certain localization accuracy could be easily obtained from the result in (6.23). For example, when the radius of the localization unit is $L = 0.5$ m, $d = 10$ m, $M = 8$, and $\sigma = 0.01$ m, the PEB $\approx 0.14$ m.

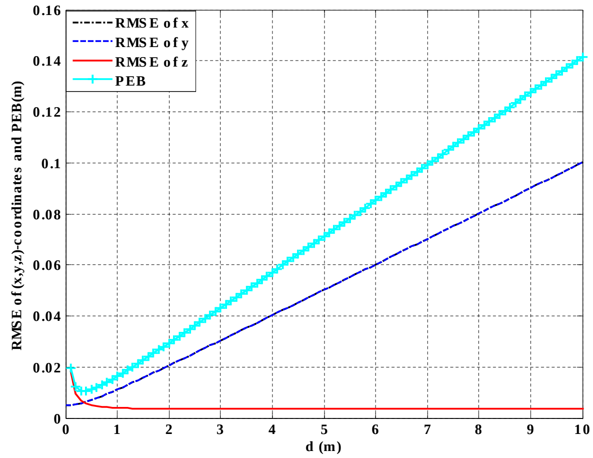


Figure 6.4: RMSE of $(x, y, z)$-coordinates and PEB ($M = 8$).

Fig. 6.4 shows the root mean-square error (RMSE) of the $(x, y, z)$-coordinates with $M = 8$. Due to symmetry of $x$ and $y$ coordinates, the RMSE values of the $x$ and $y$ coordinates are identical and they increase as $d$ increases. However, the RMSE of the $z$ coordinate decreases as the distance $d$ increases. The RMSE of $x$, $y$ and $z$ has a crossing point at $d = \frac{\sqrt{2}L}{2}$. This provides useful information about where to place the localization unit when the desired accuracies of the $x$, $y$ and $z$ coordinates are not the same. For example, to track the movement of people in an indoor area, for which the estimation accuracy of $x$ and $y$ coordinates is more important than that of the $z$ coordinate, placing the receiver unit on the ceiling might not be the best choice; instead, it might have better performance if the receiver unit is mounted on a wall.

### 6.4.2 PEB Versus Elevation Angles

We have derived the PEB for the simple case when $\mathbf{p} = [0, 0, d]^T$. Now we extend the study to the general case of $\mathbf{p} = [-d \sin\phi, 0, d\cos\phi]^T$ as shown in Fig. 6.5 mainly via simulation.

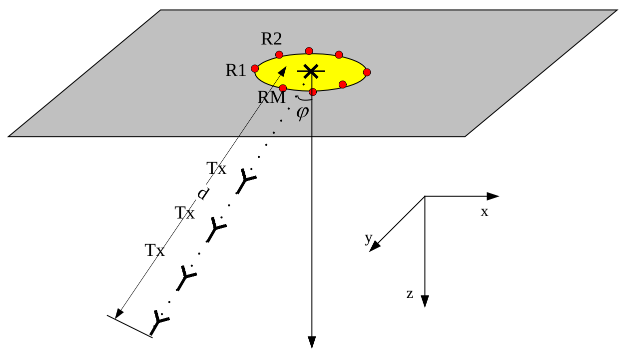


Figure 6.5: System configuration for PEB simulation when the transmitter is on a plane that is perpendicular to the receiver plane.

The following system parameters are assumed: UAA receiver geometry with $L = 0.5$ m, $\sigma = 0.01$ m, and $M = 8$. In the first simulation, the distance parameter $d = 1, 2, 3,$ and4 m, and the elevation angle is changed from 0 to $\frac{11}{12}\pi$ with a step of $\frac{\pi}{24}$. The PEB versus $d$ and $\phi$ is shown in Fig. 6.6.

In the second simulation, the setup is the same as the first simulation except that the distance $d = 4$ m is fixed. The CRLBs of the $(x, y, z)$-coordinates are plotted in Fig. 6.7.

It is observed from Fig. 6.6 that the PEB increases as the angle $\phi$ and distance $d$ increase. Fig. 6.7 shows that when the distance $d$ is fixed, the CRLB of $x$ and $y$ barely change as the elevation angle changes, but the CRLB of $z$ increases as the elevation angle increases. When $\phi < \frac{7\pi}{24}$, the CRLB of $z$ is

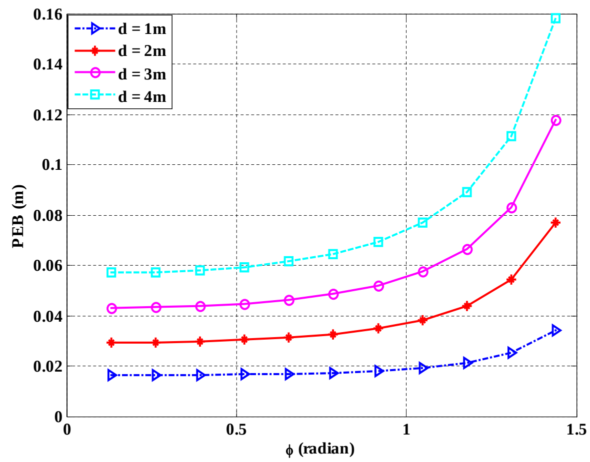


Figure 6.6: PEB versus the elevation angles and distances from the origin.

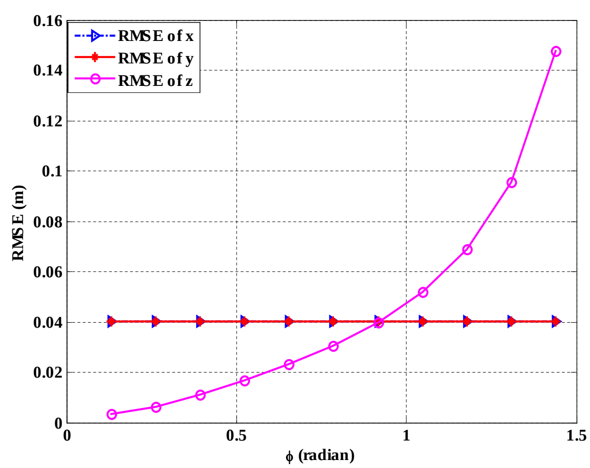


Figure 6.7: CRLB of $x, y, z$ varies as the elevation angle when $d = 4m$.

smaller than that of $x$ and $y$; when $\phi$ exceeds this angle, the CRLB of $z$ becomes greater that that of $x$ and $y$.

### 6.4.3 Average PEB

To gain a more in-depth understanding of the performance of the localization system with collocated receivers, we simulate the average PEB when the target transmitter is located at any position near the receiver unit. In the first simulation, the area in which the transmitter could be located is $10 \times 10 \times 10\ m^3$. The coordinates of $x$ and $y$ changes from $-5$ m to 5 m with a step size of 0.5 m and the $z$ coordinate is set at 1 m, 2 m, 5 m, and 10 m. The 3-D mesh plot with $z$ varying is shown in Figs. 6.8, 6.9, 6.10, and 6.11. The average PEB for each fixed $z$ value is shown in Fig. 6.12.

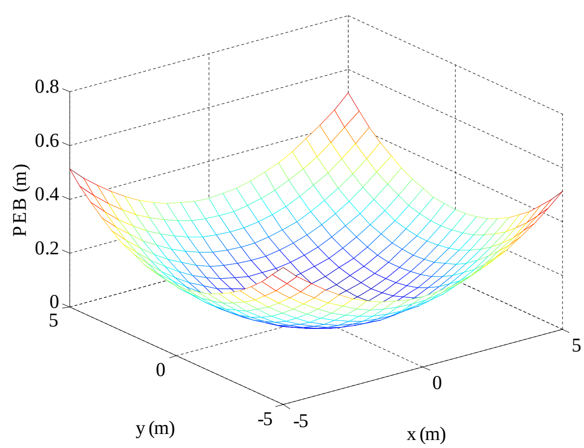


Figure 6.8: PEB when $z = 1$ m.

These plots show that when $z$ is fixed, the PEB increases as the distance between the transmitter and the receiver unit increases, as expected. However,

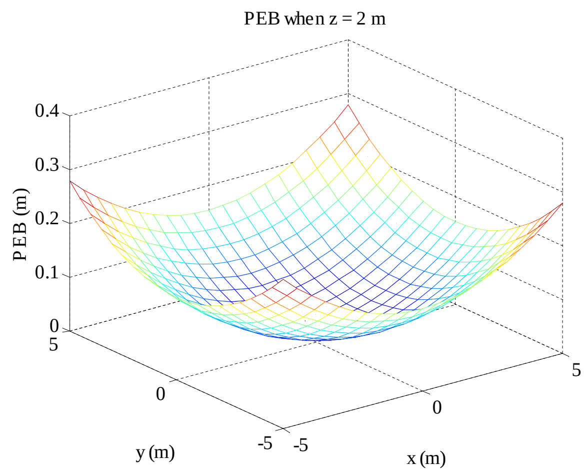


Figure 6.9: PEB when $z = 2$ m.

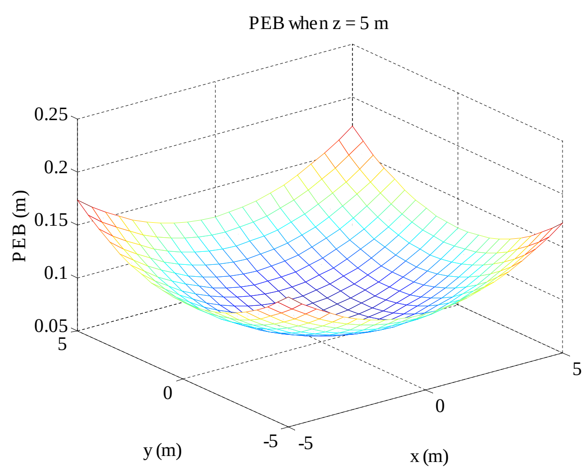


Figure 6.10: PEB when $z = 5$ m.

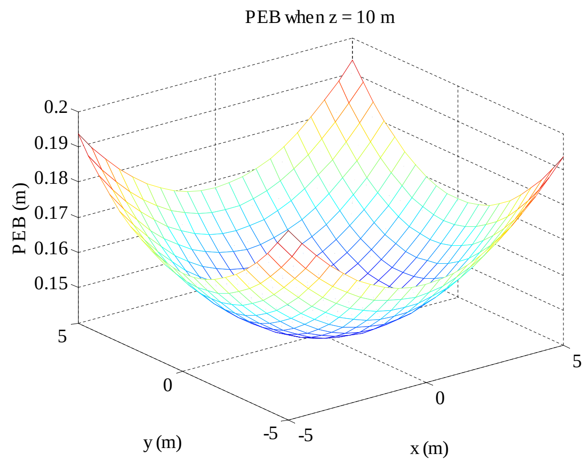


Figure 6.11: PEB when $z = 10$ m.

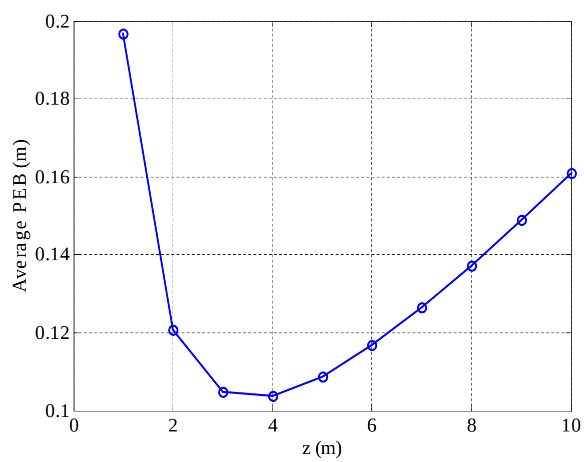


Figure 6.12: Average PEB versus $z$ in a $10 \times 10 \times 10$ $m^3$ area.

from Fig. 6.12, it is observed that the average PEB does not monotonically increase as the $z$ value increases; instead, the average PEB reaches the minimum value when $z \approx 4$ m for the configuration adopted. It shows that the PEB depends on both the elevation angle and distance between the transmitter to the receiver unit. We then shrink the simulation area to $2 \times 2 \times 10$ $m^3$ and the setup for $z$ coordinate is kept the same but the coordinates of $x$ and $y$ change from $-1$ m to 1 m with a step size of 0.1 m. The average PEB for this case is shown in Fig. 6.13, which shows that when the area is shrunk to $2 \times 2 \times 10$ $m^3$, the average PEB increases as $z$ increases. These simulation results show the average PEB is related to the size of the localization area.

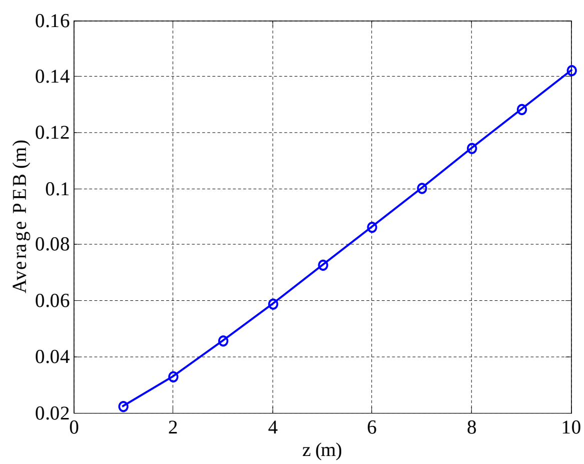


Figure 6.13: Average PEB versus $z$ in a $2 \times 2 \times 10$ $m^3$ area.

## 6.5 Experimental Results

In order to evaluate the performance of 3-D localization with collocated receivers in a realistic setting that various factors causing estimation errors are included, we have constructed a hardware and software prototype system and tested it in a laboratory environment.

### 6.5.1 Experiment Setup

The block diagram of the prototype system is shown in Fig. 6.14; it consists of a waveform generator that generates a carrier-modulated Gaussian pulse with center frequency of 4.1 GHz and $-10$ dB bandwidth of 2 GHz. The pulse duration is about 1 ns and the pulse repetition interval is 200 ns. An UWB omni-directional transmit antenna is connected to the pulse generator via a coaxial cable. The length of the coaxial cable is 50 feet, which allows the transmit antenna to be moved anywhere inside the lab. The receiver unit consists of four omni-directional antennas, wideband low-noise amplifiers, bandpass filters and a digital sampling scope.

The triggering signal from the waveform generator is used to trigger the sampling scope via a coaxial cable. The delay between the transmitter and the receivers is 28.64 ns. Therefore, the transmitter and the receivers are synchronized by subtracting this fixed reference delay.

The sampling scope has a maximum real-time sampling rate of 20 GHz (i.e., a sampling duration of 50 ps) for all four channels; therefore, the Nyquist sampling criterion is satisfied even when the signal is not down-converted to the baseband. The sampled signals are transferred to a computer through an Ethernet connection. To reduce the effect of noise, 20 sequentially received pulses are averaged.

The digital data is first upsampled to 100 GHz to increase the time resolution to 10 ps. Then it goes through a square-law device and a low-pass filter to recover the baseband pulse. The TOA between the transmitter and the four receivers are calculated using a range-estimation method that we have developed recently [12]. This method has the capability to reduce the multipath overlap effect. The position of the transmitter is calculated using the least-square method.

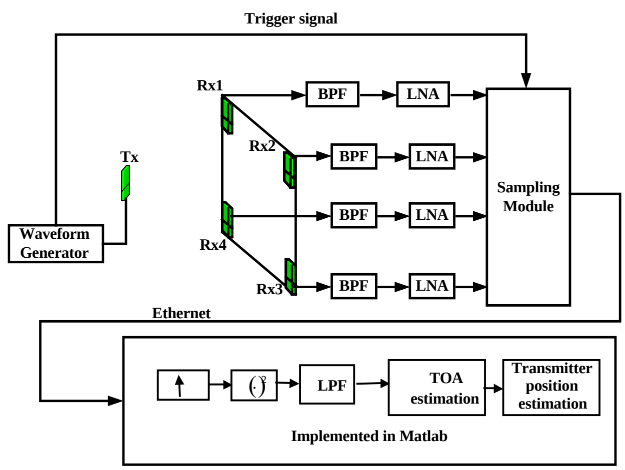


Figure 6.14: Block diagram of the experimental apparatus.

## 6.5.2 Results

Inside the lab, there are tables in the middle of the lab, metal cabinets and metal stands along the wall. The four receivers are fixed in a box on the wall.

One of the corners of the lab is designated as the origin and the coordinates of the four receivers are Rx1(153,23,177), Rx2(153,23,247), Rx3(238,23,247), Rx4(238,23,177). The four receivers are placed in the same plane, forming a rectangle of dimension 85 cm $\times$ 70 cm. The measurements are made at 36 different locations at a fixed height on the edge of a 6 m $\times$ 4.8 m rectangular with 60 cm spacing between the measurement points. The height of the measurement points is fixed at 203 cm from the floor, which ensures that the LOS component is not blocked by the table and metal stands in the room. The $x$ and $y$ coordinates of the measurement points change from 190 cm to 790 cm and from 276 cm to 756 cm, respectively. The positions of the measurement points and the receivers are shown in Fig. 6.15.

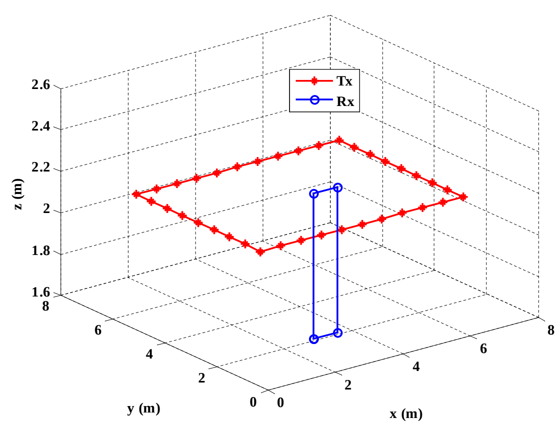


Figure 6.15: Position of the measurement points and receivers in the experiment.

At each measurement point, 100 pulses are recorded for each receiver. The average TOA between the transmitter to each receiver and the position estimates at each point are calculated. Fig. 6.16 and Fig. 6.17 show the actual and estimated positions of the 36 points for the 3-D (all $(x, y, z)$-coordinates are estimated) and 2-D (only $(x, y)$-coordinates are estimated) localization, respectively. The position error is calculated using

$$\epsilon_i = \|\hat{\mathbf{p}}_\mathbf{i} - \mathbf{p}_\mathbf{i}\| \tag{6.24}$$

where $\mathbf{p}_\mathbf{i}$ is the actual position of the $i$th measurement point and $\hat{\mathbf{p}}_\mathbf{i}$ is the estimated position of the same point.

In calculating position estimation errors for 3-D localization, the errors of all $(x, y, z)$-coordinates are considered; for 2-D localization, only the errors in $(x, y)$-coordinates are considered. The position estimation errors of each point for the 2-D and 3-D cases are shown in Fig. 6.18; the average position estimation errors are, respectively, 21.3 cm and 26.6 cm for these two cases. In order to increase the localization accuracy, one can either enlarge the dimension of the receiver unit or increase the number of receivers based on the analysis results given in Sec. 6.4.2.

## 6.6 Conclusion

We have introduced and analyzed a single-unit UWB 3-D TOA localization system. This system has several advantages such as no synchronization among the receivers is required and easy system setup. One major effort of this work is the derivation of the optimum receiver placement for this system that is not available from existing literature; we have concluded that a UAA is still the optimum receiver geometry for this single-receiver-unit localization system. An-

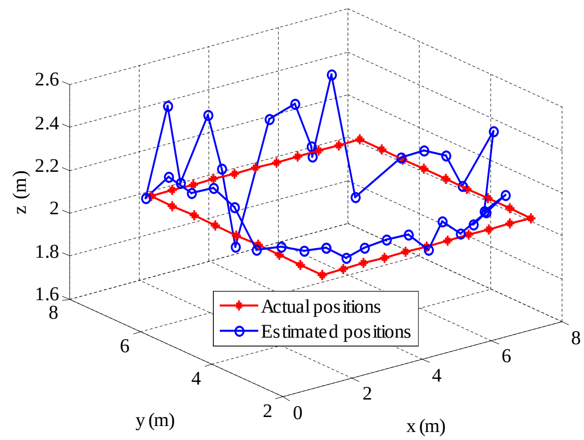


Figure 6.16: Actual and estimated positions of the measurement points for the 3-D case.

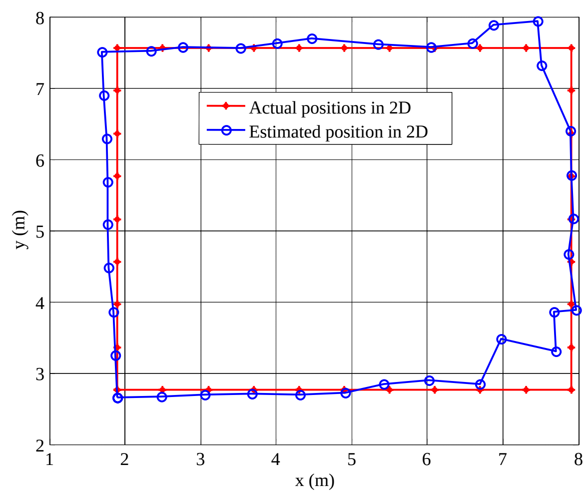


Figure 6.17: Actual and estimated positions of the measurement points for the 2-D case.

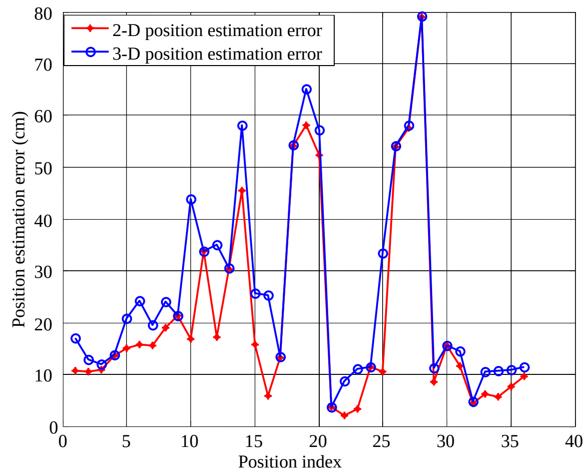


Figure 6.18: Position estimation error for the 2-D and 3-D cases.

other major effort is the derivation of the PEB as a function of the number of receivers as well as the distance between the transmitter and the receiver unit. In order to assess the performance of this system in a realistic environment, we have constructed a hardware and software prototype system, and tested it in a laboratory. The experimental results validated the theoretical results obtained in this paper. The localization accuracy can be flexibly controlled by choosing an appropriate dimension of the receiver unit and an appropriate number of receivers; with a receiver unit that has four receivers placed inside a circle of radius within 50 cm and a signal bandwidth (-10 dB) of 2 GHz, both theoretical and simulation results showed that a 3-D localization accuracy of a few decimeters is achievable for objects within 10 m of the receiver unit.

# Chapter 7 – TDOA Localization System with Multiple Collocated Receiver Units

## 7.1 Introduction

We have introduced and analyzed a single-unit UWB 3-D TOA localization system in Ch.6. This system has several advantages such as no requirement for wireless synchronization among the receivers and easy system setup. However, high precision synchronization between the transmitter and the receiver unit is still required. In a practical system implementation, many factors such as the clock jitter, clock drift, uncertainty of the processing time in the transmitter and receiver, noise, blockages, interference all can affect the synchronization accuracy and degrade the final position estimation accuracy.

To avoid the complicated wireless synchronization and keep the system setup simple, we propose a multi-unit TDOA localization system, in which each unit has a cluster of receivers placed in proximity (e.g., on a 2-D plane within a few decimeters). The receivers of each unit are synchronized via wire connections but the receivers from different units operate independently. The TDOA measurements from each unit are combined in a main processor to estimate the position of the target. This system can be viewed as a cooperative system since all the unsynchronized units cooperate to locate the target. However, it is different form the traditional cooperative localization systems where the transmitters but not the receivers are cooperative to both increase the localization accuracy and coverage [59, 60].

In this chapter, we will discuss the basic case when there are only two units in the system. The system model will be introduced first. Then the CRLB of the system will be derived under an AWGN model. The PEB of the system will be simulated under different receiver configurations. Finally, the PEB as a function of the receiver unit size will be simulated and analyzed.

## 7.2 System Model

Let us consider a system of $M$ units each with a cluster of $N$ receivers placed in proximity, shown in Fig .7.1. All the receivers in each unit are synchronized via wire connections, but different units are independent. The coordinates of all receivers are known and $\mathbf{q}_{i,j} = [x_{i,j}, y_{i,j}, z_{i,j}]^T$ represents the $(x, y, z)$-coordinates of the $j$th receiver in the $i$th unit. The unknown coordinate $\mathbf{p} = [x, y, z]^T$ of the target transmitter is to be estimated. Since the receivers in each unit are located in proximity to one another, they can be easily synchronized via wire connection.

For each unit, $N-1$ independent TDOA measurements can be obtained and a total of $M(N-1)$ TDOA measurements for the whole system are available. The target transmitter position can be estimated by combining all the TDOA measurements from all the units.

Without loss of generality, the first receiver of each unit is used as a reference receiver. The distance difference between the $j$th and the 1st receiver and the

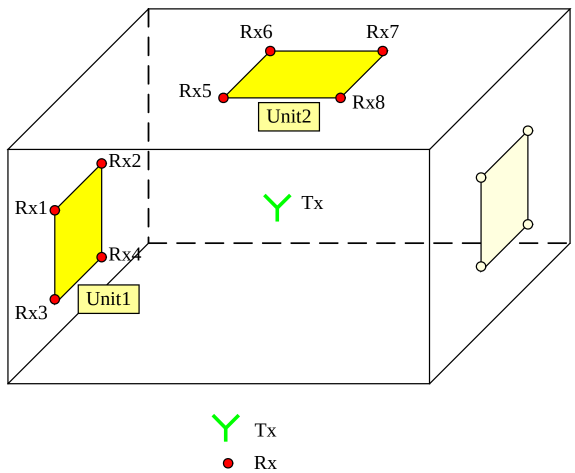


Figure 7.1: Multi-unit TDOA localization scheme.

transmitter is modeled as

$$\begin{aligned}\hat{d}_{i,j1} &= d_{i,j} - d_{i,1} + b_{i,j} - b_{i,1} + n_{i,j} - n_{i,1} \\ &= \|\mathbf{p} - \mathbf{q}_{i,j}\| - \|\mathbf{p} - \mathbf{q}_{i,1}\| + b_{i,j} - b_{i,1} + n_{i,j} - n_{i,1} \\ &= d_{i,j1} + b_{i,j1} + n_{i,j1}, i = 1, \cdots, M; j = 2, \cdots, N\end{aligned} \tag{7.1}$$

where $d_{i,j} = \|\mathbf{p} - \mathbf{q}_{i,j}\|$ is the actual distance between the $j$th receiver and the transmitter and $d_{i,1} = \|\mathbf{p} - \mathbf{q}_{i,1}\|$ is the actual distance between the 1st receiver and the transmitter, $b_{i,j}$ and $b_{i,1}$ are positive biases caused by NLOS propagation and $n_{i,j}$ is a Gaussian random variable with zero mean and variance of $2\sigma^2$. Only the LOS case is considered in this analysis; thus $b_{i,1} = 0$ and $b_{i,j} = 0$.

## 7.3 Cramér-Rao Lower Bound

The CRLB for the TDOA localization system under an AWGN model can be expressed as [27]

$$\mathbf{J}^{-1} = (\mathbf{G}\mathbf{C}^{-1}\mathbf{G}^T)^{-1} \tag{7.2}$$

where $\mathbf{J}$ is the FIM and $\mathbf{G} = [\mathbf{G_1}, \mathbf{G_2}, \cdots, \mathbf{G_M}]$ with $\mathbf{G_i} = [g_{i,21}, g_{i,31}, \cdots, g_{i,N1}]$, where

$$\mathbf{g}_{i,j1} = \frac{\mathbf{p} - \mathbf{q}_{i,j}}{\|\mathbf{p} - \mathbf{q}_{i,j}\|} - \frac{\mathbf{p} - \mathbf{q}_{i,1}}{\|\mathbf{p} - \mathbf{q}_{i,1}\|}. \tag{7.3}$$

Note that $\mathbf{G}$ is a $D \times M(N-1)$ matrix, where $D = 2, 3$ represents 2-D and 3-D localization, respectively, and $\mathbf{C}$ is the covariance matrix of $\mathbf{n}$ obtained as

$$\mathbf{C} = E[\mathbf{n}\mathbf{n}^T] \tag{7.4}$$

where $\mathbf{n} = [n_{1,21}, n_{1,31}, ..., n_{1,N1}, ..., n_{M,21}, n_{M,31}..., n_{M,N1}]^T$.

$$E[\mathbf{n}\mathbf{n}^T] = \begin{bmatrix} E[n_{1,21}n_{1,21}] & E[n_{1,21}n_{1,31}] & \cdots & E[n_{1,21}n_{M,N1}] \\ E[n_{1,31}n_{1,21}] & E[n_{1,31}n_{1,31}] & \cdots & E[n_{1,31}n_{M,N1}] \\ \vdots & \vdots & \vdots & \vdots \\ E[n_{1,N1}n_{1,21}] & E[n_{1,N1}n_{1,31}] & \ldots & E[n_{1,N1}n_{M,N1}] \\ \vdots & \vdots & \vdots & \vdots \\ E[n_{M,N1}n_{1,21}] & E[n_{M,N1}n_{1,31}] & \ldots & E[n_{M,N1}n_{M,N1}] \end{bmatrix}. \tag{7.5}$$

Two cases need to be considered for calculating the elements of the covariance matrix.

1. When the two TDOA estimation errors are from the same receiver unit;

2. When the two TDOA estimation errors are from different receiver units.

For case 1 and when $j \neq k$:

$$
\begin{aligned}
E[n_{i,j1}n_{i,k1}] &= E[(n_{i,j} - n_{i,1})(n_{i,k} - n_{i,1})] \\
&= E[n_{i,j}n_{i,k}] - E[n_{i,j}n_{i,1}] - E[n_{i,1}n_{i,k}] + E[n_{i,1}n_{i,1}] \\
&= 0 - 0 - 0 + \sigma^2 \\
&= \sigma^2.
\end{aligned} \tag{7.6}
$$

For case 1 and when $j = k$:

$$
\begin{aligned}
E[n_{i,j1}n_{i,j1}] &= E[(n_{i,j} - n_{i,1})(n_{i,j} - n_{i,1})] \\
&= E[n_{i,j}n_{i,j}] - E[n_{i,j}n_{i,1}] - E[n_{i,1}n_{i,j}] + E[n_{i,1}n_{i,1}] \\
&= 2\sigma^2.
\end{aligned} \tag{7.7}
$$

For case 2, when the TDOA estimation errors are from different units, the distance difference estimates are independent and we have

$$
\begin{aligned}
E[n_{i,j1}n_{h,k1}] &= E[(n_{i,j} - n_{i,1})(n_{h,k} - n_{h,1})] \\
&= E[n_{i,j}n_{h,k}] - E[n_{i,j}n_{h,1}] - E[n_{i,1}n_{h,k}] + E[n_{i,1}n_{h,1}] \\
&= 0.
\end{aligned} \tag{7.8}
$$

Therefore, the covariance matrix $\mathbf{C}$ is obtained as

$$\mathbf{C} = \begin{bmatrix} \mathbf{C1} & \mathbf{0} & \cdots & \mathbf{0} \\ \mathbf{0} & \mathbf{C1} & \cdots & \mathbf{0} \\ \vdots & \vdots & \ddots & \vdots \\ \mathbf{0} & \mathbf{0} & \cdots & \mathbf{C1} \end{bmatrix}. \tag{7.9}$$

where $\mathbf{C1}$ is an $(N-1) \times (N-1)$ matrix expressed as

$$\mathbf{C1} = \begin{bmatrix} 2\sigma^2 & \sigma^2 & \cdots & \sigma^2 \\ \sigma^2 & 2\sigma^2 & \cdots & \sigma^2 \\ \vdots & \vdots & \ddots & \vdots \\ \sigma^2 & \sigma^2 & \cdots & 2\sigma^2 \end{bmatrix}. \tag{7.10}$$

The FIM is calculated as

$$\begin{aligned} \mathbf{J} &= \mathbf{G}\mathbf{C}^{-\mathbf{1}}\mathbf{G}^T \\ &= \mathbf{G_1}\mathbf{C_1}\mathbf{G_1}^T + \mathbf{G_2}\mathbf{C_1}\mathbf{G_2}^T + \cdots + \mathbf{G_M}\mathbf{C_1}\mathbf{G_M}^T \\ &= \mathbf{J_1} + \mathbf{J_2} + \cdots + \mathbf{J_M}. \end{aligned} \tag{7.11}$$

From (7.11), it is noted that the FIM of the whole system equals to the summation of the FIM of each receiver unit.

## 7.4 Simulation Results

From the CRLB derivation, the localization accuracy is affected by the FIM of each receiver unit, which in turn is affected by the following factors: (a)

The TDOA estimation accuracy; (b) The number of units; (c) The size of each unit; (d) The receiver configuration in each unit; (e) The number of receivers in each unit; and (f) The placement of all the units. Many factors can affect the final estimation accuracy of the system and it is hard to find an optimum setup. In this section, we will analyze the localization performance through the PEB simulation under certain conditions. For simplicity, following conditions are assumed.

1) There are two units each having four receivers;

2) All receivers in a unit are put on a plane forming a square;

3) The standard deviation of the distance difference estimate is set to be 1 cm;

4) The simulation area is 10 m $\times$ 10 m $\times$ 5 m;

5) The size of each receiver unit is 1 m $\times$ 1 m.

Three configurations with the two units located at different places are simulated. The 2-D and 3-D PEB of the localization system for each configuration will be analyzed. The three configurations are shown in Fig. 7.2, Fig. 7.3 and Fig. 7.4.

In configuration I, two units are put in the middle of the two side walls. The coordinates of the four receivers in the first unit are $\mathbf{q}_{1,1} = [0, 4.5, 2]^T, \mathbf{q}_{1,2} = [0, 5.5, 2]^T, \mathbf{q}_{1,3} = [0, 5.5, 3]^T]$ and $\mathbf{q}_{1,4} = [0, 4.5, 3]^T$, and the coordinates of the receivers in the second unit are $\mathbf{q}_{2,1} = [10, 4.5, 2]^T, \mathbf{q}_{2,2} = [10, 5.5, 2]^T, \mathbf{q}_{2,3} = [10, 5.5, 3]^T$ and $\mathbf{q}_{2,4} = [10, 4.5, 3]^T$.

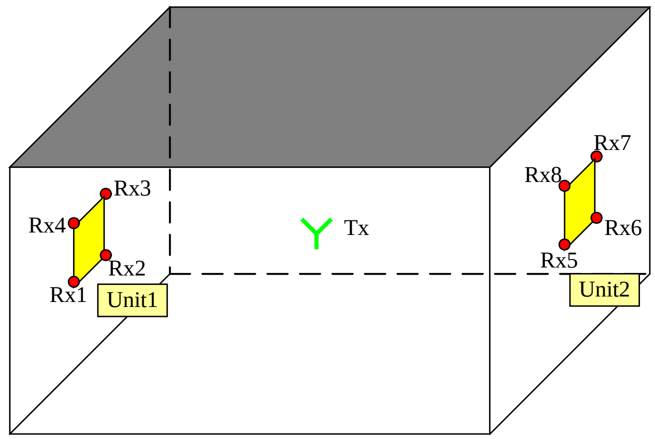


Figure 7.2: Configuration I.

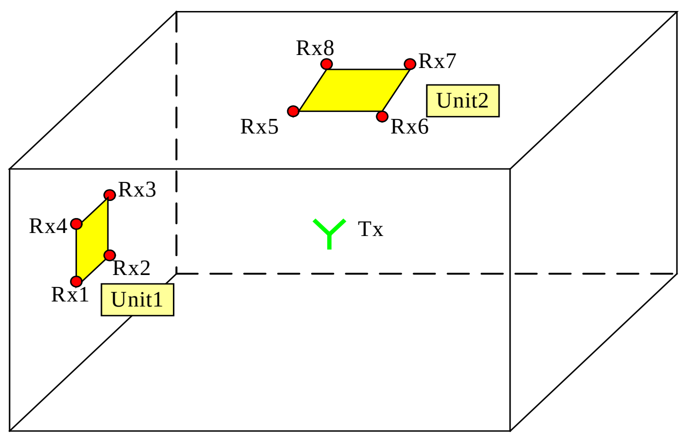


Figure 7.3: Configuration II.

In configuration II, one of the units is placed on the ceiling and the other is located in the middle of the side wall as in configuration I. The coordinates of the four receivers in the first unit is the same as in configuration I; the coordinates of the four receivers in the second receiver unit are $\mathbf{q}_{2,1} = [4.5, 4.5, 2]^T$, $\mathbf{q}_{2,2} = [5.5, 5.5, 2]^T$, $\mathbf{q}_{2,3} = [5.5, 5.5, 3]^T]$ and $\mathbf{q}_{2,4} = [4.5, 5.5, 3]^T$.

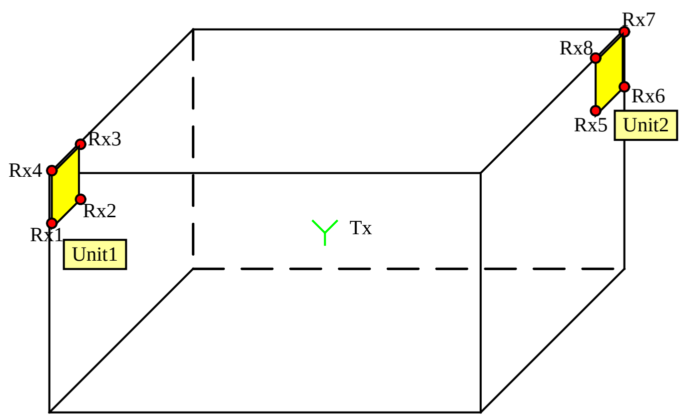


Figure 7.4: Configuration III.

In configuration III, the two units are placed on the corner of the two side walls. The coordinates of the four receivers in the first unit are $\mathbf{q}_{1,1} = [0, 0, 4]^T$,$\mathbf{q}_{1,2} = [0, 1, 4]^T$,$\mathbf{q}_{1,3} = [0, 1, 5]^T$, and $\mathbf{q}_{1,4} = [0, 0, 5]^T$; the coordinates of the other four receivers in the second units are $\mathbf{q}_{2,1} = [10, 9, 4]^T$,$\mathbf{q}_{2,2} = [10, 10, 4]^T$,$\mathbf{q}_{2,3} = [10, 10, 5]^T$, and $\mathbf{q}_{2,4} = [10, 9, 5]^T$.

### 7.4.1 PEB for 2-D Localization

The $(x, y)$-coordinates changes from $-5$ m to 5 m with a step of 0.5 m and the $z$ coordinate varies from 0 m to 5 m with a step of 1 m. The 3-D mesh plot of the 2-D PEB with $z = 1$ m and $z = 2$ m are shown in Figs. 7.5 and 7.6. The average PEB for each fixed $z$ value is shown in Fig. 7.7.

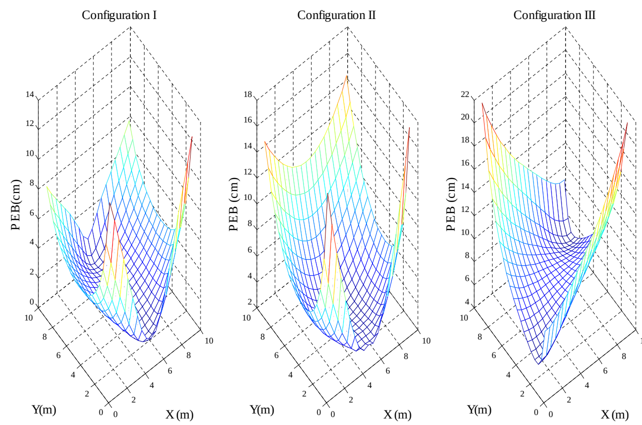


Figure 7.5: PEB for $(x, y)$- coordinates when $z = 1$ m.

It is observed from Fig. 7.5 and Fig. 7.6 that the system has the worst localization accuracy in the four corners for all three configurations. Fig. 7.7 shows that Configuration III has the worst performance in terms of the average PEB; Configuration II has slight better accuracy than Configuration I when $z$ is smaller than 4 m, but Configuration I has a better accuracy when $z$ is greater than 4 m. The average PEB for the 2-D localization is smaller than 10 cm for Configuration I.

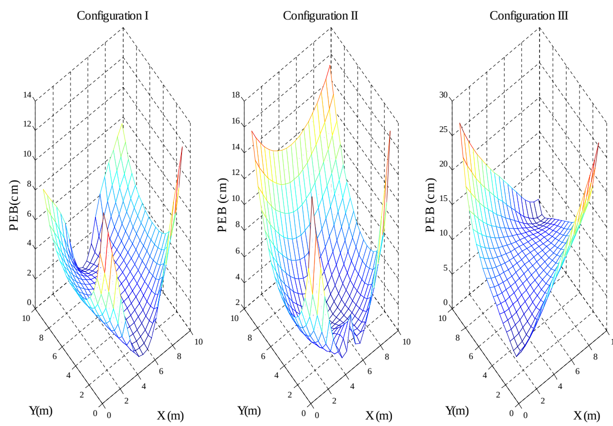


Figure 7.6: PEB for $(x, y)$- coordinates when $z = 2$ m.

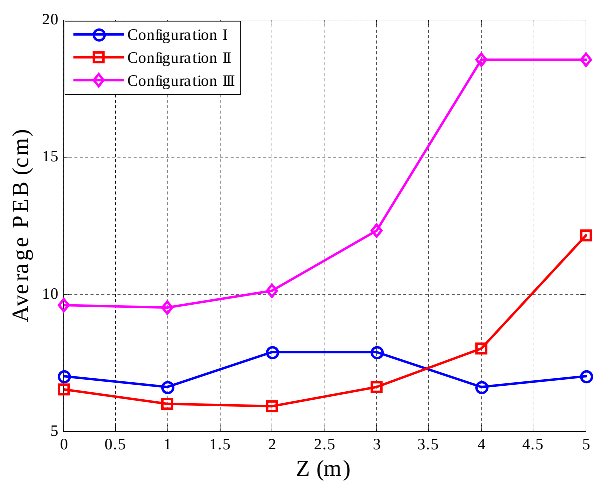


Figure 7.7: Average PEB versus $z$ in a $10 \times 10 \times 5\ m^3$ area.

### 7.4.2 PEB for 3-D Localization

The PEB for the 3-D localization is simulated and analyzed for the three configurations under the same conditions as the 2-D case. The 3-D mesh plot of the PEB for the 3-D localization with $z = 1, 2$ m is shown in Figs. 7.8 and 7.9. The average 3-D PEB for each fixed $z$ value is shown in Fig. 7.10.

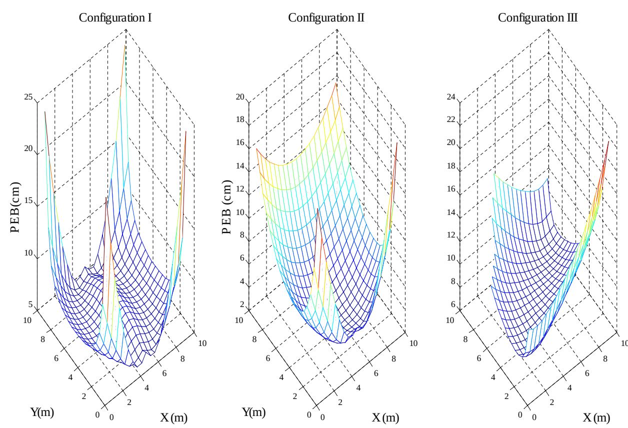


Figure 7.8: PEB for x,y when $z = 1$ m.

The simulation results are similar to the 2-D case: Configuration III has the worst position estimation accuracy among the three configurations. Configuration II has a slightly better accuracy when $z = 1, 2, 3$ m but has a worst accuracy for the other $z$ values compared to configuration I. The average PEB is smaller than 20 cm for all three configurations. For configuration I, the PEB is smaller than 10 cm.

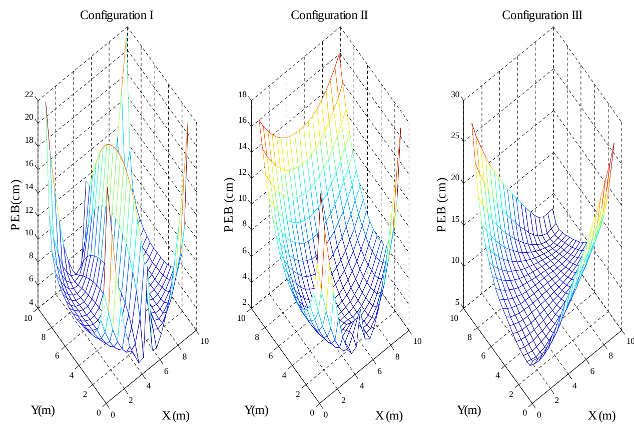


Figure 7.9: PEB when $z = 2$ m.

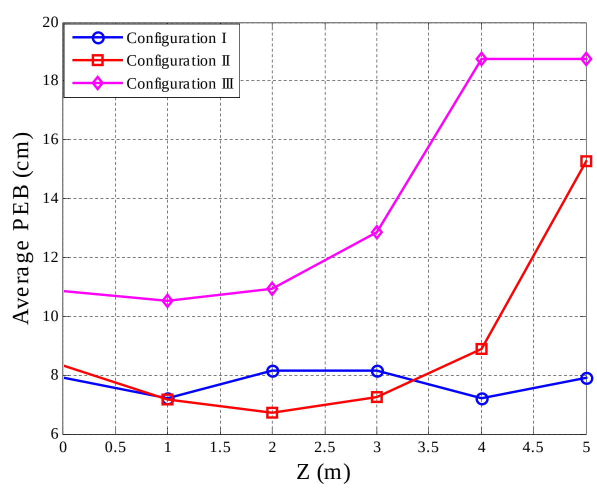


Figure 7.10: Average PEB versus $z$ in a $10 \times 10 \times 5\ m^3$ area.

### 7.4.3 PEB as a Function of Receiver Unit Size

From the 2-D and 3-D PEB analysis, Configuration I has a slightly better and more stable performance than the other two configurations. In this section, assuming that the unit placement is fixed, we analyze the PEB as a function of the receiver unit size. Both units are square with a side length of $L$ m varies from 0.2 m to 2 m with a step of 0.2 m. Other simulation setups are the same as the previous simulations. The PEB for 2-D and 3-D localization versus the unit size is simulated. The simulation results are shown in Figs. 7.11, 7.12, 7.13 and 7.14.

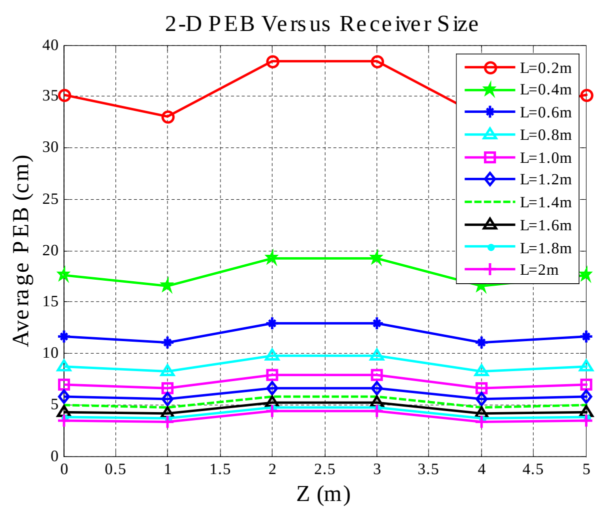


Figure 7.11: Average PEB for 2-D localization vs the receiver unit size.

The simulation results show that both the 2-D and 3-D average PEB decrease as the unit size increases. The localization accuracy is dramatically increased when the side length of the unit increases from 0.2 m to 0.4 m, where the average PEB decreases about 17 cm and 20 cm for the 2-D and 3-D cases. However, the

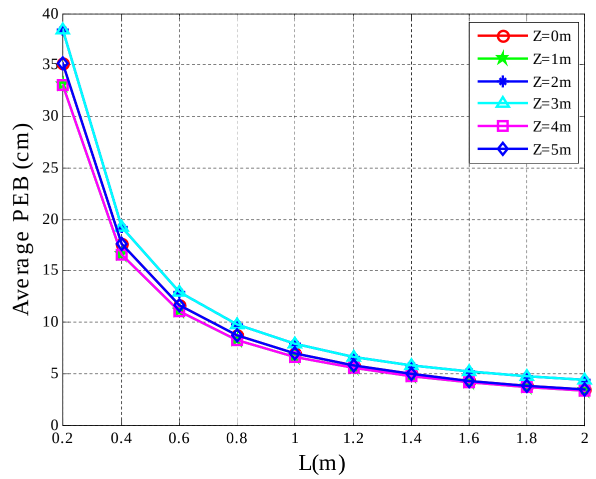


Figure 7.12: Average PEB for 2-D localization vs the receiver unit size.

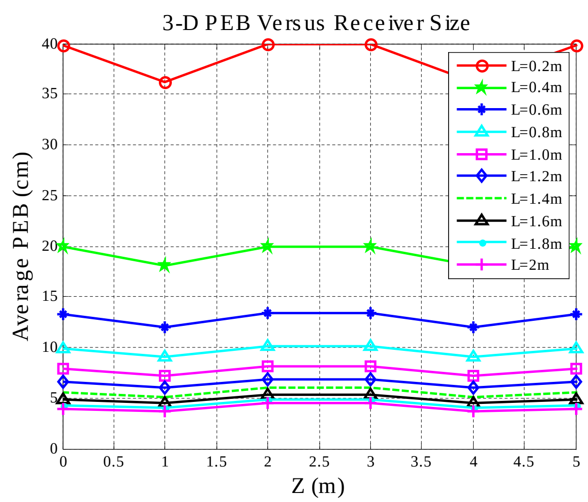


Figure 7.13: Average PEB for 3-D localization vs the receiver unit size.

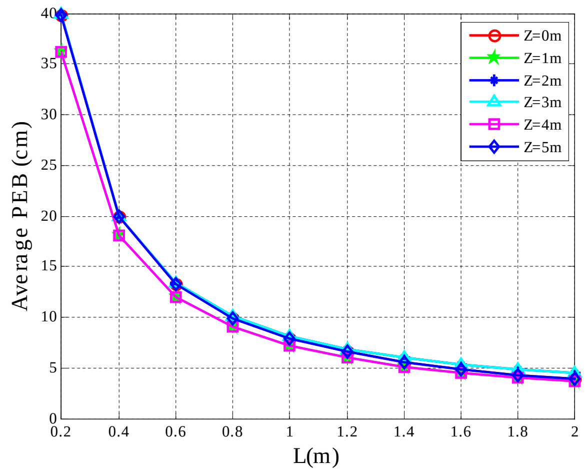


Figure 7.14: Average PEB for 3-D localization vs the receiver unit size.

improvement rate of the accuracy slows down as the unit size increases. The average PEB improvement is less than 1 cm when the unit size is increased from 1.8 m × 1.8 m m to 2 m × 2 m. For both 2-D and 3-D localization, when the size of the unit is greater than 0.8 m × 0.8 m, the average PEB is less than 10 cm. If the unit is increased to 2 m × 2 m, both the average PEB for 2-D and 3-D localization are less than 5 cm. In practical applications, the unit should be made as small as possible to meet the accuracy requirement.

## 7.5 Conclusion

We have proposed and analyzed a multiple-unit UWB 3-D TDOA localization system. This system has several advantages such as no wireless synchronization among the receivers and transmitter is required, simple system design and easy system setup. The CRLB of the system has been derived. The PEB of the system for three different configurations are simulated and analyzed. The relation between the PEB versus the unit size is analyzed. It is observed that the average PEB decreases as the unit size increases. The simulation and theoretical analysis of this system provide a good guidance for practical system design.

Form the simulation, it is observed that this system has the potential to achieve a decimeter localization accuracy. Because of the simple system setup, it can be applied for most localization applications like monitoring seniors at home or tracking assets in indoor environments.

# Chapter 8 – Conclusion and Future Work

## 8.1 Conclusion

This dissertation focuses on developing algorithms and architectures of UWB localization systems with different accuracy requirements and system complexity constraints.

First, a wired centimeter-accurate UWB localization system is developed. The technical challenges toward achieving a centimeter localization accuracy are investigated. A new range estimation algorithm is proposed to reduce the effect of pulse-overlap. Both simulation and experiment results show that the new method can effectively reduce the pulse-overlap effect and achieve centimeter accuracy in a multipath environment.

Secondly, we analyze the effect of the receiver geometric configurations on the TDOA localization system performance. We derive a function of the GDOP versus the number of receivers, and simulate the PEB with different signal bandwidths and different numbers of receivers using the UWB indoor distance measurement error model. This analysis is useful to guide a practical system design in optimizing the choices of signal bandwidth and the number of receivers to achieve a certain localization accuracy.

Thirdly, we develop a wireless localization system with centimeter accuracy. A two-step synchronization algorithm with picoseconds accuracy is presented. This system is tested in a laboratory environment and the experiment results show that this system has the potential to achieve centimeter accuracy.

Fourthly, in order to reduce the system complexity, we investigate an UWB 3-D localization scheme with a single cluster of receivers. This scheme employs the TOA technique and there is no requirement of wireless synchronization among the receivers. A hardware and software prototype that works in the 3.1-5.1 GHz range is constructed and tested in a laboratory environment. An average position estimation error of smaller than 3 decimeter was achieved by the experiment system.

Finally, in order to further reduce system complexity, a new TDOA localization scheme with multiple receiver units is proposed. In this scheme, each unit operates with its own clock, and no synchronization between the transmitter and receivers is required, allowing a very simple transmitter design. The performance of this system is also analyzed analytically.

## 8.2 Future Work

In the future, more studies are needed to optimize the wireless localization system design and make the system more stable. In addition, NLOS is another major factor that significantly decreases the localization accuracy, which is not investigated in this dissertation. NLOS detection and mitigation algorithms should be investigated and implemented in future localization systems. For the multi-unit TDOA localization system, more investigations and tests are needed to evaluate its localization accuracy.

# Bibliography

[1] S. Krishnan, and P. Sharma, G. Zhang. and O. H. Woon, "A UWB based localization system for indoor robot navigation," in *Proc. ICUWB'07*, Sep. 2007, pp. 77–82.

[2] Zafer Sahinoglu, Sinan Gezici, and Ismail Guvenc,"*Ultra-wideband Positioning Systems: Theoretical limits, Ranging Algorithms, and Protocols*." Cambridge University Press, 2008.

[3] R. C. Qiu, H. Liu, and X. Shen, "Ultra-wideband for multiple access communications," *IEEE Commun. Mag.*, vol. 43, no. 4, pp. 80–87, Feb. 2005.

[4] X. Shen, M. Guizani, R.C. Qiu, and T. Le-Ngoc, " *Ultra-Wideband wireless communications and networks*." John Wiley and Sons Ltd, 2006.

[5] Ubisense, Cambridge, U.K., Hardware datasheet, 2006. [Online]. Available: `Http://www.ubisense.net/SITE/UPLOAD/Document/Tech-Docs/Ubisense_hardware_datasheet_May_2006.pdf`.

[6] Multispectral solutions, Sappire DART positioning system. [Online]. Available: `http://www.multispectral.com/sapphiredart.html`

[7] Time domain corporation website. [Online]. Available: `http://timedomain.com/products/p350.pdf`

[8] C. Meier, A. Terzis, and S. Lindenmeier, "A robust 3D high precision radio location system," in proc. *IEEE MTT-S Int. Microw. Symp. Dig.*, 2007, pp. 397–400.

[9] A. Fujii, H. Sekiguchi, M. Asai, S. Kurashima, H. Ochiai, and R.Kohno, "Impulse radio UWB positioning system," in *Proc. IEEE Radio Wireless Symp.*, 2007, pp. 55–58.

[10] M.R. Mahfouz, C. Zhang, B.C. Merkl, M.J. Kuhn, and A.E. Fathy, "Investigation of high-accuracy indoor 3-D positioning using UWB technology," *IEEE Trans. Microw. Theory Tech.*, vol. 56, no. 6, pp. 1316–1330, Jun. 2008.

[11] C. Zhang, M. J. Kuhn, B. C. Merkl, A. E. Fathy, and M. R. Mahfouz, "Real-time noncoherent UWB positioning radar with millimeter range accuracy: Theory and Experiment," *IEEE Trans. Microw. Theory Tech.*, vol. 58, Issue. 1, pp. 9–20, Jan. 2010.

[12] R. Ye, S. Redfield, H. Liu, " High-Precision Indoor UWB Localization: Technical Challenges and Method, " in *Proc. ICUWB'10*, Sep. 2010, pp. 509–512.

[13] Y. Zhou, Y. L. Guan, C. L. Law, and C. Xu, "High-resolution UWB ranging based on phase-only correlator," in *Proc. ICUWB'07*, Sep. 2007, pp. 100–104.

[14] Z. N. Low, J.H. Cheong, C.L. Law, W. T. Ng, and Y.J. Lee, "Pulse detection algorithm for line-of-sight (LOS) UWB ranging applications," *IEEE Antennas and Wireless Propaga. Lett.,* vol. 4, pp. 63–67, June 2005.

[15] C. Falsi, D. Dardari, L. Mucchi, and M. Z. Win, "Time of arrival estimation for UWB localizers in realistic environments," *EURASIP J. Applied Signal Processing,* vol. 2006, pp. 1–13, July 2006.

[16] R. Yarlagadda, I. Ali, N. Al-Dhahir, and J. Hershey, "GPS GDOP metric," *IEE Proceedings - Radar, Sonar and Navigation,* pp. 259–264, Oct. 2000.

[17] B. Yang and J. Scheuing, "Cramer-Rao bound and optimum sensor array for source localization from time differences of arrival," in *Proc. IEEE ICASSP'05*, May 2005, pp. 961–964.

[18] B. Yang, "Different sensor placement strategies for TDOA based localization," in *Proc. ICASSP'07*, Apr. 2007, pp. 1093–1096.

[19] J. Schroeder, S. Galler, K. Kyamakya, and K. Jobmann, "Practical considerations of optimal three-dimensional indoor localization," in *Proc. MFI'06*, Dec. 2006, pp. 439–443.

[20] R. Ye and H. Liu, " UWB TDOA localization system: receiver configuration analysis, " in *Proc. ISSSE'10*, Sep. 2010, pp. 1–4.

[21] R. Ye and H. Liu, "Ultra-wideband localization with collocated receivers," in *Proc. ICUWB'11*, Sep. 2011, pp. 155–159.

[22] Federal Communications Commission, "First Report and Order 02-48", Feb. 2002.

[23] M.Z. Win and R.A. Scholtz, "Impulse radio: How it works," *IEEE Commun. Lett.*, vol. 2, no. 2, pp. 36–38, 1998

[24] Federal Communications Commission, "Part 15 - Radio Frequency Devices," Feb. 2006. [Online]. Available: http://www.fcc.gov/oet/info/rules/part15/part15-2-16-06.pdf

[25] G. Breed, "A summary of FCC rules for ultra wideband communications," in *High Frequency Electronics,* Jan.2005. [Online]. Available: http://www.highfrequencyelectronics.com/Archives/Jan05/HFE0105_Tutorial.pdf

[26] Y. Qi, " Wireless geolocation in a non-line-of-sight environment." Ph.D dissertation, Princeton University, USA, Dec.2004.

[27] H.V. Poor,"*An Introduction to Signal Detection and Estimation*." New York: Springer-Verlag, 1994.

[28] S. Baek, R. Ye, C. Hu, S. Redfield, H. Liu, T. Hayes, P. Chiang, "Preliminary study of indoor ultrawideband localization for at-home patient monitoring," in *Proc. 2010 AMA-IEEE Medical Technology Conf. on Individualized Healthcare*, Mar. 2010.

[29] J.S. McLean, H. Foltz, and R. Sutton, "Conditions for direction-independent distortion in UWB antennas," *IEEE Trans. Antennas Propag.*, vol. 54, pp. 3178–3183, Nov. 2006.

[30] G. Wang and W. Kong, "Angle-dependent pulse distortion in UWB radiation and its impact on UWB impulse communications," *Electron. Lett.*, vol. 41, pp. 1360–1361, Dec. 2005.

[31] Fractus Optimised Antennas for wireless Devices,[Online]. Available: http://www.fractus.com/sales_documents/FR05-S1-P-0-107/DS_FR05-S1-P-0-107.pdf

[32] Z.N. Chen, "UWB antennas: Design and application," in *Proc. Int. Conf. Inform., Commun., Signal Process.*, Dec. 2007, pp. 1–5.

[33] J.S. McLean, H. Foltz, and R. Sutton, "Pattern descriptors for UWB antennas," *IEEE Trans. Antennas Propag.*, vol. 53, pp. 553–559, Jan. 2005.

[34] Y. Takeuchi, Y. Shimizu, and Y. Sanada, "Experimental examination of antennas for a UWB positioning system," in *Proc. ICUWB'05*, Sep. 2005, pp. 269–274.

[35] A. Taha and K.M. Chugg, "On designing the optimal template waveform for UWB impulse radio in the presence of multipath," in *Proc. IEEE ICUWB'02*, Aug. 2002, pp. 41–45.

[36] J. McLean, H.D. Foltz, and R. Sutton, "The effect of frequency-dependent radiation pattern on UWB antenna performance," in *Proc. Int. Symp. Antenna and Propagation*, June 2004, pp. 2540–2543.

[37] R.C. Qiu, C. Zhou, and Q. Liu, "Physics-based pulse distortion for ultra-wideband signals," *IEEE Trans. Veh. Technol.*, vol. 54, no. 5, pp. 1546–1555, Sep. 2005.

[38] X. H. Li, G. Wang, and W. Kong, "On the selection of template pulse waveform in UWB impulse communications," in *Proc. IEEE Int. Symp. Antennas and Propagation*, July 2006, pp. 1311–1314.

[39] A. Sibille, S. Bories, R. D'Errico, and C. Roblin; "UWB antenna performance evaluation from the communication system point of view," in *Proc. ISWCS'06*, Sep. 2006, pp. 417–422.

[40] Y. Shen and M.Z. Win, "Effect of path-overlap on localization accuracy in dense multipath environments," in *Proc. IEEE Int. Conf. Commun.*, Mar. 2008, pp. 4197–4202.

[41] M. Kuhn, Cemin Zhang , B. Merkl, Depeng Yang , Yazhou Wang , M. Mahfouz, and A. Fathy, " High accuracy UWB localization in dense indoor environments," in *Proc. ICUWB'08*, Sep. 2008, pp. 129–132.

[42] D. Dardari, A. Conti, U. Ferner, A. Giorgetti, and M.Z. Win, "Ranging with ultrawide bandwidth signals in multipath environments," *Proceedings of the IEEE,* vol. 97, no. 4, pp. 404–426, Mar. 2009.

[43] S. Gezici, Z. Tian, G. B. Giannakis, H. Kobayashi, A. F. Molisch, H. V. Poor, and Z. Sahinoglu, "Localization via ultra-wideband radios: a look at positioning aspects for future sensor networks," *IEEE Signal Processing Mag.*, vol. 22, no. 4, pp. 70–84, Jul. 2005.

[44] C. Knapp and G. Garter, "The generalized correlation method for estimation of time delay," *IEEE Trans. Acoustics, Speech, and Signal Processing*, vol. 24, pp. 320–327, Aug. 1976.

[45] W.H. Foy, "Position-location solutions by Taylor-series estimation," *IEEE Trans. Aerosp. Electron. Syst.*, vol. AES-12, pp. 187–194, Mar. 1976.

[46] Y.T. Chan and K.C. Ho, "A simple and efficient estimator for hyperbolic location," *IEEE Trans. Signal Processing*, vol. 42, pp. 1905–1915, Aug. 1994.

[47] B. Alavi and K. Pahlavan, "Modeling of the TOA-based distance measurement error using UWB indoor radio measurements," *IEEE Commun. Lett.*, vol. 10, no. 4, pp. 275–277, June 2006.

[48] Institue for Inforcomm Research,Singapore, 2010. [Online]. Available: `http://www.fusionworld.sg/factsheets/Enterprise/ULTRA.pdf`.

[49] W. W. Ji and Z. Liu, " Optimum geometry selection in mobile sensor networks," in *Proc. Int. Conf. Commun. Technol.*, May 2006, vol.4, pp. 14–19.

[50] K. C. Ho and Luis M. Vicente, " Sensor allocation for source localization with decoupled range and bearing estimation," *IEEE. Trans. Signal Process.*, Vol. 56, pp. 5773–5789, Dec. 2008.

[51] D. Jourdan, D. Dardari, and M. Win, "Position error bound for UWB localization in dense cluttered environments," *IEEE Trans. Aerosp. Electron. Syst.*, vol. 44, pp. 613–628, Apr. 2008.

[52] S.M. Kay, " *Fundamentals of Statistical Signal Processing, Volume I: Estimation Theory.*" Prentice Hall, 1993

[53] Michael P. Knapp, " Sines and cosines of angles in arithmetic progression" *Mathematics Magazine*, Vol. 82, pp. 371-372. Dec. 2009.

[54] Johannes Huschle,"Data acquisition in a wireless UWB-localization prototype system," Master Thesis, University of Applied Science Offenburg, Germany, 2010.

[55] National Semiconductor Corporation, "ADC08D1500 High Performance, Low Power, Dual 8-Bit, 1.5GSPS A/D Converter." [Online]. Available:`http://www.ti.com/lit/ds/snas316f/snas316f.pdf`.

[56] Seungjin Baek, "Receiver synchronization for UWB TDOA localization," Master Thesis, Oregon State University, US, 2010.

[57] H. Matsumoto1, H. Kusano1, T. Morokuma1, and Ken Sakamura, "Numerical and Experimental Investigation of TDOA-Based Positioning System by Ultra-Wideband Impulse Radio," in *Proc. of IEEE Conf. Wireless Sensors and Sensor Networks (WiSNet).*, Jan. 2011, pp. 25–28.

[58] K. Mizugaki, "Accurate Wireless Location/Communication System With 22-cm Error Using UWB-IR," in *Proc. of IEEE Radio and Wireless Symposium*, Jan. 2007, pp. 455–458.

[59] U. Ferner, H. Wymeersch, and M.Z.Win, "Cooperative anchor-less localization for large dynamic networks," in *Proc. ICUWB'08*, Sep. 2008, pp. 181–185.

[60] H. Wymeersch, J. Lien, and M.Z. Win, "Cooperative Localization in Wireless Networks," *Proceedings of the IEEE*, vol. 97, Issue. 2, pp. 427–450, Feb. 2009.

[61] R. Bhatia, *Positive definite matrix*, Princeton Series in Applied Mathematics, 2007.

[62] C.Bellusci, G.Janssen, J.Yan, and C.Tiberius, "Model of distance and bandwidth dependency of TOA-based UWB ranging error," in *Proc. IEEE ICUWB'08*, vol. 3, pp. 193–196, Sep. 2008.